UNDERSTANDING LATENT CORRELATION-BASED MULTIVIEW LEARNING AND SELF-SUPERVISION: AN IDENTIFIABILITY PERSPECTIVE

Anonymous authors
Paper under double-blind review

ABSTRACT

Multiple views of data, both naturally acquired (e.g., image and audio) and artificially produced (e.g., via adding different noise to data samples), have proven useful in enhancing representation learning. Natural views are often handled by multiview analysis tools, e.g., (deep) canonical correlation analysis [(D)CCA], while the artificial ones are frequently used in self-supervised learning (SSL) paradigms, e.g., `BYOL` and `Barlow Twins`. Both types of approaches often involve learning neural feature extractors such that the embeddings of data exhibit high cross-view correlations. Although intuitive, the effectiveness of correlation-based neural embedding is mostly empirically validated. This work aims to understand latent correlation maximization-based deep multiview learning from a latent component identification viewpoint. An intuitive generative model of multiview data is adopted, where the views are different nonlinear mixtures of shared and private components. Since the shared components are view/distortion-invariant, representing the data using such components is believed to reveal the identity of the samples effectively and robustly. Under this model, latent correlation maximization is shown to guarantee the extraction of the shared components across views (up to certain ambiguities). In addition, it is further shown that the private information in each view can be provably disentangled from the shared using proper regularization design. A finite sample analysis, which has been rare in nonlinear mixture identifiability study, is also presented. The theoretical results and newly designed regularization are tested on a series of tasks.

1 INTRODUCTION

One pillar of unsupervised representation learning is multiview learning. Extracting shared information from multiple "views" (e.g., image and audio) of data entities has been considered a major means to fend against noise and data scarcity. A key computational tool for multiview learning is *canonical correlation analysis* (CCA) (Hotelling, 1936). The classic CCA seeks linear transformation matrices such that transformed views are maximally correlated. A number of works studied nonlinear extensions of CCA; see kernel CCA in (Lai & Fyfe, 2000) and *deep learning-based CCA* (DCCA) in (Andrew et al., 2013; Wang et al., 2015). DCCA and its variants were shown to largely outperform the classical linear CCA in many tasks.

In recent years, a series of *self-supervised learning* (SSL) paradigms were proposed. These SSL approaches exhibit a lot of similarities with DCCA approaches, except that the "views" are noisy data "augmenented" from the original clean data. To be specific, different views are generated by distorting data—e.g., using rotating, cropping, and/or adding noise to data samples (Dosovitskiy et al., 2015; Gidaris et al., 2018; Chen et al., 2020; Grill et al., 2020). Then, neural encoders are employed to map these artificial views to embeddings that are highly correlated across views. This genre—which will be referred to as artificial multiview SSL (AM-SSL)—includes a number of empirically successful frameworks, e.g., `BYOL` (Grill et al., 2020) and `Barlow Twins` (Zbontar et al., 2021).

Notably, many DCCA-type approaches and AM-SSL approaches involve (explicitly or implicitly) searching for highly correlated representations from multiple views, using neural networks as view-

specific feature extractors (encoders). The empirical success of DCCA and AM-SSL bears an important research question: *How to understand the effectiveness of cross-view correlation-based deep learning criteria?* Furthermore, how to use such understanding to design theory-backed learning criteria to serve various purposes?

Intuitively, it makes sense that many DCCA and AM-SSL paradigms involve latent correlation maximization in their loss functions, as such loss functions lead to similar/identical representations from different views—which identifies view-invariant essential information that is often identity-revealing. However, beyond intuitions, theoretical understanding has been lacking. In this work, we aim at understanding latent correlation-based DCCA and AM-SSL from a nonlinear mixture learning viewpoint—and using such understanding to serve various learning tasks, e.g., downstream clustering, cross-view translation, and cross-sample generation. Our detailed contributions lie in the following aspects:

(i) Understanding Latent Correlation Maximization - Shared Component Identification. We start with a concept that has been advocated in many multiview learning works. In particular, the views are nonlinear mixtures of shared and private latent components; see, e.g., (Huang et al., 2018; Lee et al., 2018; Wang et al., 2016). The shared components are distortion/view invariant and identity-revealing. The private components and view-specific nonlinear mixing processes determine the different appearances of the views. In this work, we show that maximizing the correlation of latent representations extracted from different views leads to identification of the ground-truth shared components. This result may shed some light on the effectiveness of a suite of DCCA and AM-SSL paradigms.

(ii) Imposing Additional Constraints - Private Component Identification. Using the understanding to latent correlation maximization-type loss functions in DCCA and AM-SSL, we take a step further. We show that with carefully imposed constraints, the private components in the views can also be identified, under reasonable assumptions. Learning private components can facilitate tasks such as cross-view and cross-sample data generation (Huang et al., 2018; Lee et al., 2018).

(iii) Finite-Sample Analysis. Most existing unsupervised nonlinear mixture identification works, e.g., those from the nonlinear independent component analysis (ICA) literature (Hyvarinen & Morioka, 2016; 2017; Hyvarinen et al., 2019; Khemakhem et al., 2020; Locatello et al., 2020; Gresele et al., 2020), are based on infinite data. This is perhaps because finite sample analysis for unsupervised learning is generally much more challenging relative to supervised cases—and there is no existing "universal" analytical tools. In this work, we provide sample complexity analysis for the proposed *unsupervised* multiview learning criterion. In particular, we characterize how the performance of extracting latent components shared across views scales with the number of samples.

(iv) Practical Implementation. Based on the theoretical understanding, we propose a latent correlation-maximization based multiview learning criterion for extracting both the shared components and private components. To realize the criterion, a notable innovation is a minimax neural regularizer that serves for extracting the private components. The regularizer shares the same purpose of some known independence promoters (e.g., *Hilbert-Schmidt Independence Criterion* (HSIC) (Gretton et al., 2005a)) but is arguably easier to implement using stochastic gradient algorithms.

Notation. The notations used in this work are summarized in the supplementary material.

2 Background: Latent Correlation in DCCA and AM-SSL

In this section, we briefly review some deep multiview learning paradigms that use latent correlation maximization and its close relatives.

2.1 Latent Correlation Maximization in DCCA

DCCA methods aim at extracting common information from multiple views of data samples. Such information is expected to be informative and essential in representing the data.

• **DCCA.** The objective of DCCA can be summarized as follows (Andrew et al., 2013):

$$\underset{\boldsymbol{f}^{(1)},\boldsymbol{f}^{(2)}}{\text{maximize}} \ \mathrm{Tr}\left(\mathbb{E}\left[\boldsymbol{f}^{(1)}\left(\boldsymbol{x}^{(1)}\right)\boldsymbol{f}^{(2)}\left(\boldsymbol{x}^{(2)}\right)^{\top}\right]\right), \quad \text{s.t. } \mathbb{E}\left[\boldsymbol{f}^{(q)}\left(\boldsymbol{x}^{(q)}\right)\boldsymbol{f}^{(q)}\left(\boldsymbol{x}^{(q)}\right)^{\top}\right] = \boldsymbol{I}, \quad (1)$$

where $\boldsymbol{x}^{(q)} \in \mathbb{R}^{M_q} \sim \mathcal{D}_q$ is a data sample from view q for $q = 1, 2$, $\mathcal{D}_q$ is the underlying distribution of the qth view, $\boldsymbol{f}^{(1)} : \mathbb{R}^{M_1} \to \mathbb{R}^D$ and $\boldsymbol{f}^{(2)} : \mathbb{R}^{M_2} \to \mathbb{R}^D$ are two neural networks. CCA was found particularly useful in terms of fending against unknown and strong view-specific (private) interference (see theoretical supports in (Bach & Jordan, 2005; Ibrahim & Sidiropoulos, 2020)). Such properties were also observed in DCCA research (Wang et al., 2015), while theoretical analysis is mostly elusive.

An equivalent representation of (1) is as follows

$$\underset{\boldsymbol{f}^{(1)},\boldsymbol{f}^{(2)}}{\text{minimize}} \ \mathbb{E}\left[\left\|\boldsymbol{f}^{(1)}(\boldsymbol{x}^{(1)}) - \boldsymbol{f}^{(2)}(\boldsymbol{x}^{(2)})\right\|_2^2\right], \quad \text{s.t. } \mathbb{E}\left[\boldsymbol{f}^{(q)}\left(\boldsymbol{x}^{(q)}\right)\boldsymbol{f}^{(q)}\left(\boldsymbol{x}^{(q)}\right)^\top\right] = \boldsymbol{I}, \tag{2}$$

which is expressed from *latent component matching* perspective. Both the correlation maximization form in (1) and the component matching form in (2) are widely used in the literature. As we will see in our proofs, although the former is popular in the literature (Andrew et al., 2013; Wang et al., 2015; Chen et al., 2020), the latter is handier for theoretical analysis.

• **Slack Variable-Based DCCA.** In (Benton et al., 2017) and (Lyu & Fu, 2020), a deep multiview learning criterion is used:

$$\underset{\boldsymbol{f}^{(q)}}{\text{minimize}} \sum_{q=1}^{2} \mathbb{E}\left[\left\|\boldsymbol{f}^{(q)}(\boldsymbol{x}^{(q)}) - \boldsymbol{g}\right\|^2\right], \text{ s.t. } \mathbb{E}[|g_i|^2] = 1, \ \mathbb{E}[g_i g_j] = 0. \tag{3}$$

The slack variable $\boldsymbol{g}$ represents the *common* latent embedding learned from the two views. Conceptually, this is also latent correlation maximization (or latent component matching). To see this, assume that there exists $\boldsymbol{f}^{(q)}(\boldsymbol{x}^{(q)}) = \boldsymbol{g}$. The criterion amounts to learning $[\boldsymbol{f}^{(1)}(\boldsymbol{x}^{(1)})]_k = [\boldsymbol{f}^{(2)}(\boldsymbol{x}^{(2)})]_k$—which has the maximally attainable correlation.

2.2 Latent Correlation Maximization/Component Matching in AM-SSL

Similar to DCCA, the goal of AM-SSL is also to find identity-revealing embeddings of data samples without using labels. The idea is often realized via intentionally distorting the data to create multiple artificial views. Then, the encoders are require to produce highly correlated (or closely matched) embeddings from such views. In AM-SSL, the views $\boldsymbol{x}^{(1)}$ and $\boldsymbol{x}^{(2)}$ are different augmentations (e.g., by adding noise, cropping, and rotation) of the sample $\boldsymbol{x}$.

• **Barlow Twins.** The most recent development, namely, the `Barlow Twins` network (Zbontar et al., 2021) is appealing since it entails a succinct implementation. Specifically, the `Barlow Twins` network aims to learn a *single* encoder $\boldsymbol{f} : \mathbb{R}^M \to \mathbb{R}^D$ for two distorted views. The cost function is as follows:

$$\underset{\boldsymbol{f}}{\text{minimize}} \ \sum_{i=1}^{D} (1 - C_{ii})^2 + \lambda \sum_{i=1}^{D}\sum_{j\neq i}^{D} C_{ij}^2, \ \text{ where } C_{ij} = \frac{\mathbb{E}\left[[\boldsymbol{f}(\boldsymbol{x}^{(1)})]_i [\boldsymbol{f}(\boldsymbol{x}^{(2)})]_j\right]}{\sqrt{\mathbb{E}[[\boldsymbol{f}(\boldsymbol{x}^{(1)})]_i^2]}\sqrt{\mathbb{E}[[\boldsymbol{f}(\boldsymbol{x}^{(2)})]_j^2]}}.$$

When the learned embeddings are constrained to have zero mean, i.e., $\mathbb{E}\left[\boldsymbol{f}(\boldsymbol{x}^{(q)})\right] = \boldsymbol{0}$, C_{ij} is the cross-correlation between $\boldsymbol{f}(\boldsymbol{x}^{(1)})$ and $\boldsymbol{f}(\boldsymbol{x}^{(2)})$. Note that the normalized representation of cross-correlation in C_{ij} is equivalent to the objective in (1) with the orthogonality constraints.

• **BYOL.** The `BYOL` method (Grill et al., 2020) uses a cross-view matching criterion that can be distilled as follows:

$$\underset{\boldsymbol{f}^{(1)},\boldsymbol{f}^{(2)}}{\text{minimize}} \ \mathbb{E}\left[\left\|\overline{\boldsymbol{f}}^{(1)}(\boldsymbol{x}^{(1)}) - \overline{\boldsymbol{f}}^{(2)}(\boldsymbol{x}^{(2)})\right\|_2^2\right] \tag{4}$$

where $\overline{\boldsymbol{f}}^{(q)}(\cdot)$ means that the output of the network is normalized. In `BYOL`, the networks are constructed in a special way (e.g., part of $\boldsymbol{f}^{(2)}$'s weights are moving averages of the correspond part of $\boldsymbol{f}^{(1)}$'s weights). Nonetheless, the cross-view matching perspective is still very similar to that in latent component matching in (2).

• **SimSiam.** The loss function of `SimSiam` (Chen & He, 2021) has a similar structure as that of `BYOL`, but with a Siamese network, which, essentially, is also latent component matching.

3 UNDERSTANDING LATENT CORRELATION MAXIMIZATION

In this section, we offer understandings to latent correlation maximization (and latent component matching) from an unsupervised nonlinear multiview mixture identification viewpoint. We will also show that such understanding can help improve multiview learning criteria to serve different purposes, e.g., cross-view and cross-sample data generation.

3.1 MULTIVIEW AS NONLINEAR MIXTURES OF PRIVATE AND SHARED COMPONENTS

We consider the following multiview generative model:

$$\boldsymbol{x}_\ell^{(1)} = \boldsymbol{g}^{(1)}\left(\begin{bmatrix}\boldsymbol{z}_\ell \\ \boldsymbol{c}_\ell^{(1)}\end{bmatrix}\right),\ \boldsymbol{x}_\ell^{(2)} = \boldsymbol{g}^{(2)}\left(\begin{bmatrix}\boldsymbol{z}_\ell \\ \boldsymbol{c}_\ell^{(2)}\end{bmatrix}\right), \tag{5}$$

where $\boldsymbol{x}_\ell^{(q)} \in \mathbb{R}^{M_q}$ is the ℓth sample of the qth view for $q = 1, 2$, $\boldsymbol{z}_\ell \in \mathbb{R}^D$ is the shared component across views, and $\boldsymbol{c}_\ell^{(q)} \in \mathbb{R}^{D_q}$ represents the private information of the qth view—which are the ℓth samples of continuous random variables denoted by $\boldsymbol{z} \in \mathbb{R}^D$, $\boldsymbol{c}^{(q)} \in \mathbb{R}^{D_q}$, respectively. In addition, $\boldsymbol{g}^{(q)}(\cdot) : \mathbb{R}^{D+D_q} \to \mathbb{R}^{M_q}$ is an *invertible* and *smooth* nonlinear transformation, which is unknown.

Generative Models of Multiview Analysis. We should mention that the intuition that multiview data consists of shared and private components are widely used; see, e.g., (Huang et al., 2018; Lee et al., 2018; Wang et al., 2016; Gundersen et al., 2019). However, explicit generative models were only considered in limited theory-oriented works. The model in (5) can be understood as a nonlinear generalization of the linear CCA model in (Ibrahim & Sidiropoulos, 2020), where the views are modeled as $\boldsymbol{x}_\ell^{(q)} = \boldsymbol{A}^{(q)}[\boldsymbol{z}_\ell^\top, (\boldsymbol{c}_\ell^{(q)})^\top]^\top$ for $q = 1, 2$. In (Lyu & Fu, 2020), a special type of nonlinear model, namely, the post-nonlinear mixture model, was analyzed. There, the model is $\boldsymbol{x}_\ell^{(q)} = \boldsymbol{g}^{(q)}(\boldsymbol{A}^{(q)}[\boldsymbol{z}_\ell^\top, (\boldsymbol{c}_\ell^{(q)})^\top]^\top)$, where $\boldsymbol{g}^{(q)}(\boldsymbol{y})$ applies a nonlinear distortion to each element of $\boldsymbol{y}$ *individually*. However, post-nonlinear models are much less general compared to our model in (5)—where $\boldsymbol{g}^{(q)}(\boldsymbol{y})$ nonlinearly distorts all elements of $\boldsymbol{y}$ *jointly* in an unknown way. More recently, under the context of AM-SSL, the work in (von Kügelgen et al., 2021) considered a multiview generative model that is similar to our model, but the views share the *same* generative nonlinear function, i.e., $\boldsymbol{x}_\ell^{(q)} = \boldsymbol{g}([\boldsymbol{z}_\ell^\top, (\boldsymbol{c}_\ell^{(q)})^\top]^\top)$. This assumption restricts the applicability of the model to scenarios where the two views are generated using exactly the same nonlinear distortions, which may be less flexible. Our model in (5) subsumes the models in (Ibrahim & Sidiropoulos, 2020; Lyu & Fu, 2020; von Kügelgen et al., 2021) as its special cases.

Learning Goals. Our interest lies in extracting $\boldsymbol{z}_\ell$ and $\boldsymbol{c}_\ell^{(q)}$ (up to certain ambiguities) from the views in an unsupervised manner. In particular, we hope to answer under what conditions these latent components can be identified—and to what extent. As mentioned, $\boldsymbol{z}_\ell$ is view/distortion-invariant and thus should be identity-revealing. The ability of extracting it may explain DCCA and AM-SSL's effectiveness. In addition, the identification of $\boldsymbol{c}_\ell^{(q)}$ and the mixing processes may help generate data in different views.

3.2 A LATENT CORRELATION-BASED LEARNING CRITERION

Given observations from both views $\{\boldsymbol{x}_\ell^{(1)}, \boldsymbol{x}_\ell^{(2)}\}_{\ell=1}^N$ generated from (5), we aim to understand how latent correlation maximization (or latent component matching) helps with our learning goals. To this end, we consider the following problem criterion:

$$\underset{\boldsymbol{f}^{(1)},\boldsymbol{f}^{(2)}}{\text{maximize}}\ \mathrm{Tr}\left(\frac{1}{N}\sum_{\ell=1}^N \boldsymbol{f}_{\mathrm{S}}^{(1)}\left(\boldsymbol{x}_\ell^{(1)}\right)\boldsymbol{f}_{\mathrm{S}}^{(2)}\left(\boldsymbol{x}_\ell^{(2)}\right)^\top\right) \tag{6a}$$

$$\text{subject to } \boldsymbol{f}^{(q)} \text{ for } q = 1, 2 \text{ are invertible}, \tag{6b}$$

$$\frac{1}{N}\sum_{\ell=1}^N \boldsymbol{f}_{\mathrm{S}}^{(q)}\left(\boldsymbol{x}_\ell^{(q)}\right)\boldsymbol{f}_{\mathrm{S}}^{(q)}\left(\boldsymbol{x}_\ell^{(q)}\right)^\top = \boldsymbol{I},\ \frac{1}{N}\sum_{\ell=1}^N \boldsymbol{f}_{\mathrm{S}}^{(q)}\left(\boldsymbol{x}_\ell^{(q)}\right) = \boldsymbol{0},\ q = 1, 2, \tag{6c}$$

$$\boldsymbol{f}_{\mathrm{S}}^{(q)}\left(\boldsymbol{x}_\ell^{(q)}\right) \perp\!\!\!\perp \boldsymbol{f}_{\mathrm{P}}^{(q)}\left(\boldsymbol{x}_\ell^{(q)}\right),\ q = 1, 2, \tag{6d}$$

where $\boldsymbol{f}^{(q)}: \mathbb{R}^{M_q} \to \mathbb{R}^{D+D_q}$ for $q=1,2$ are the feature extractors of view q. We use the notations

$$\boldsymbol{f}_{\mathrm{S}}^{(q)}\left(\boldsymbol{x}_\ell^{(q)}\right) = \left[\boldsymbol{f}^{(q)}\left(\boldsymbol{x}_\ell^{(q)}\right)\right]_{1:D}, \ \boldsymbol{f}_{\mathrm{P}}^{(q)}\left(\boldsymbol{x}_\ell^{(q)}\right) = \left[\boldsymbol{f}^{(q)}\left(\boldsymbol{x}_\ell^{(q)}\right)\right]_{D+1:D+D_q}, \ q=1,2,$$

to denote the encoder-extracted shared and private components for each view, respectively. Note that designating the first D dimensions of the encoder outputs to represent the shared information is without loss of generality, since the permutation ambiguity is intrinsic.

The correlation maximization objective is reminiscent of the criteria of learning paradigms such as `DCCA` and `Barlow Twins`. In addition, under the constraints in (6), the objective function is also equivalent to shared component matching that is similar to those used by `BYOL` and `SimSiam`, i.e.,

$$\max_{\boldsymbol{f}^{(q)}} \operatorname{Tr}\left(\frac{1}{N}\sum_{\ell=1}^{N} \boldsymbol{f}_{\mathrm{S}}^{(1)}\left(\boldsymbol{x}_\ell^{(1)}\right) \boldsymbol{f}_{\mathrm{S}}^{(2)}\left(\boldsymbol{x}_\ell^{(2)}\right)^\top\right) \Longleftrightarrow \min_{\boldsymbol{f}^{(q)}} \frac{1}{N}\sum_{\ell=1}^{N} \left\| \boldsymbol{f}_{\mathrm{S}}^{(1)}\left(\boldsymbol{x}_\ell^{(1)}\right) - \boldsymbol{f}_{\mathrm{S}}^{(2)}\left(\boldsymbol{x}_\ell^{(2)}\right)\right\|_2^2.$$

To explain the criterion, note that we have a couple of goals that we hope to achieve with $\boldsymbol{f}_{\mathrm{S}}^{(q)}$ and $\boldsymbol{f}_{\mathrm{P}}^{(q)}$. First, the objective function aims to maximize the latent correlation of the learned shared components, i.e., $\boldsymbol{f}_{\mathrm{S}}^{(q)}$. This is similar to those in DCCA and AM-SSL, and is based on the belief that the shared information should be identical across views. Second, in (6d), we ask $\boldsymbol{f}_{\mathrm{S}}^{(q)}$ and $\boldsymbol{f}_{\mathrm{P}}^{(q)}$ to be statistically independent for $q=1,2$. This promotes the disentanglement of the shared and private parts of each encoder. View-specific components are often considered as interference or noise, both in DCCA and AM-SSL, and thus being independent to the essential information. Third, the invertibility constraint in (6b) is to ensure that the latent and the ambient data can be constructed from each other—which is often important in unsupervised learning, for avoiding trivial solutions. The orthogonality and zero-mean constraints in (6c) are used to make the correlation metric meaningful. In particular, if the learned components are not zero-mean, the learned embeddings may not capture "co-variations" but dominated by some constant terms.

We should mention that we design the criterion in (6) to achieve two goals simultaneously, namely, identifying the shared components and separating the shared from the private components. If one only aims to extract the shared information, then there is no need to have (6d) or the splitting of $\boldsymbol{f}_{\mathrm{S}}^{(q)}$ and $\boldsymbol{f}_{\mathrm{P}}^{(q)}$, as will be shown in Theorem 1. If this is the case, the criterion in (6) is even closer to the DCCA and AM-SSL formulations mentioned in the previous section.

3.3 Theoretical Understanding

To offer rigorous theoretical analyses for (6), we make the following assumption:

Assumption 1 (Group Independence) *Under (5), the samples $\boldsymbol{z}_\ell$ and $\boldsymbol{c}_\ell^{(q)}$ are realizations of shared and private continuous latent random variables $\boldsymbol{z}$, $\boldsymbol{c}^{(q)}$ for $q=1,2$, whose joint distributions satisfy the following:*

$$\boldsymbol{z} \sim p(\boldsymbol{z}), \ \boldsymbol{c}^{(q)} \sim p(\boldsymbol{c}^{(q)}), \ \boldsymbol{z} \in \mathcal{Z}, \ \boldsymbol{c}^{(q)} \in \mathcal{C}_q, \quad p(\boldsymbol{z}, \boldsymbol{c}^{(1)}, \boldsymbol{c}^{(2)}) = p(\boldsymbol{z})p(\boldsymbol{c}^{(1)})p(\boldsymbol{c}^{(2)}), \tag{7}$$

where $\mathcal{Z} \subseteq \mathbb{R}^D$, $\mathcal{C}_q \subseteq \mathbb{R}^{D_q}$ are the continuous supports of $p(\boldsymbol{z})$ and $p(\boldsymbol{c}^{(q)})$, respectively.

We have the following theorem in terms of learning the shared components.

Theorem 1 *(**Shared Component Extraction**) Under the generative model in (5) and Assumption 1, consider the population form in (6) (i.e., $N=\infty$). Assume that the considered constraints hold over all $\boldsymbol{x}^{(q)} \in \mathcal{X}_q$ for $q=1,2$, where $\mathcal{X}_q = \{\boldsymbol{x}^{(q)} | \boldsymbol{x}^{(q)} = \boldsymbol{g}^{(q)}([\boldsymbol{z}^\top, (\boldsymbol{c}^{(q)})^\top]^\top), \ \forall \boldsymbol{z} \in \mathcal{Z}, \forall \boldsymbol{c}^{(q)} \in \mathcal{C}_q\}$. Denote $\widehat{\boldsymbol{f}}^{(q)}$ as any solution of (6). Also assume that the first-order derivative of $\widehat{\boldsymbol{f}}^{(q)} \circ \boldsymbol{g}^{(q)}$ exists. Then, we have $\widehat{\boldsymbol{z}} = \widehat{\boldsymbol{f}}_{\mathrm{S}}^{(q)}\left(\boldsymbol{x}^{(q)}\right) = \boldsymbol{\gamma}(\boldsymbol{z})$ no matter if (6d) is enforced or not, where $\boldsymbol{\gamma}(\cdot): \mathbb{R}^D \to \mathbb{R}^D$ is a certain invertible function.*

A remark is that $\widehat{\boldsymbol{z}} = \boldsymbol{\gamma}(\boldsymbol{z})$ has all the information of $\boldsymbol{z}$ due to the invertibility of $\boldsymbol{\gamma}(\cdot)$. Theorem 1 clearly indicates that latent correlation maximization/latent component matching can identify the

view/distortion-invariant information contained in multiple views under unknown nonlinear distortions. This result may serve as theoretical support the effectiveness of the aforementioned DCCA and AM-SSL schemes, which all advocate latent correlation maximization/latent component matching as part of their objectives. Note that Theorem 1 also indicates that if one only aims to extract view-invariant information, the constraint in (6d) is not needed. In the next theorem, we show that our designed constraint in (6d) can help disentangle the shared and private components:

Theorem 2 *(***Private Component Extraction***) Under the same conditions as in Theorem 1, also assume that (6d) is enforced. Then, we further have* $\widehat{\boldsymbol{c}}^{(q)} = \widehat{\boldsymbol{f}}_{\mathrm{P}}^{(q)}\left(\boldsymbol{x}^{(q)}\right) = \boldsymbol{\delta}^{(q)}\left(\boldsymbol{c}^{(q)}\right)$*, where* $\boldsymbol{\delta}^{(q)}(\cdot) : \mathbb{R}^{D_q} \to \mathbb{R}^{D_q}$ *is a certain invertible function.*

Note that separating $\boldsymbol{z}$ and $\boldsymbol{c}^{(q)}$ may be used for other tasks such as cross-view translation (Huang et al., 2018; Lee et al., 2018) or content/style disaggregation (von Kügelgen et al., 2021).

The above theorems are based on the so-called *population case* (with $N = \infty$ and the $\mathcal{X}_q$ observed). This is similar to the vast majority of provable nonlinear ICA/factor disentanglement literature; see (Hyvarinen & Morioka, 2016; Hyvarinen et al., 2019; Locatello et al., 2020; Khemakhem et al., 2020). It is of interest to study the finite sample case. In addition, most of these works assumed that the learning function $\boldsymbol{f}^{(q)}$ is a universal function approximator. In practice, considering $\boldsymbol{f}^{(q)} \in \mathcal{F}$, where $\mathcal{F}$ is a certain restricted function class that may have mismatches with $\boldsymbol{g}^{(q)}$'s function class, is meaningful. To proceed, we assume $D_1 = D_2$ and $M = M_1 = M_2$ for notation simplicity and:

Assumption 2 *Assume the following conditions hold:*

(a) We have $\boldsymbol{g}^{(q)} \in \mathcal{G}$ *and learn* $\boldsymbol{f}^{(q)}$ *from* $\mathcal{F}$*, where the function classes* $\mathcal{F}$ *and* $\mathcal{G}$ *are third-order differentiable and bounded.*

(b) The Rademacher complexity (Bartlett & Mendelson, 2002) of $\mathcal{F}' = \{\boldsymbol{f}_d : \mathbb{R}^M \to \mathbb{R} | \boldsymbol{f}_d(\boldsymbol{x}) = [\boldsymbol{f}(\boldsymbol{x})]_d, \boldsymbol{f} \in \mathcal{F}\}$ *is bounded by* $\mathfrak{R}_N$ *given* N *samples.*

(c) Define $\mathcal{G}^{-1} = \left\{\boldsymbol{u} : \mathbb{R}^M \to \mathbb{R}^{D+D_1} | \boldsymbol{u}_{\mathrm{S}}(\boldsymbol{x}) = \boldsymbol{\gamma}(\boldsymbol{z}), \boldsymbol{u}_{\mathrm{S}}(\boldsymbol{x}) = [\boldsymbol{u}(\boldsymbol{x})]_{1:D}\right\}$ $\forall \boldsymbol{x} \in \mathcal{X}_q$ *and any invertible* $\boldsymbol{\gamma}(\cdot)$*. There exists* $\boldsymbol{f} \in \mathcal{F}$ *such that* $\sup_{\boldsymbol{x} \in \mathcal{X}_q} \|\boldsymbol{f}_{\mathrm{S}}(\boldsymbol{x}) - \boldsymbol{u}_{\mathrm{S}}(\boldsymbol{x})\|_2 \leq \nu$*.*

(d) Any third-order partial derivative of $[\boldsymbol{h}^{(q)}(\boldsymbol{x})]_d = [\boldsymbol{f}^{(q)} \circ \boldsymbol{g}^{(q)}(\boldsymbol{x})]_d$ *resides in* $[-C_d, C_d]$ *for all* $\boldsymbol{x} \in \mathcal{X}_q$*. In addition,* $[\boldsymbol{c}^{(q)}]_j \in [-C_p, C_p]$ *with* $0 < C_p < \infty$ *for* $j \in [D_q]$*.*

Theorem 3 *(***Sample Complexity***) Under the generative model in (5), Assumption 1 and the suite of conditions in Assumption 2, assume that* $(\boldsymbol{x}_\ell^{(1)}, \boldsymbol{x}_\ell^{(2)})$ *for* $\ell = 1, \ldots, N$ *are i.i.d. samples of* $(\boldsymbol{x}^{(1)}, \boldsymbol{x}^{(2)})$*. Denote* $\widehat{\boldsymbol{f}}^{(q)}$ *as any solution of (6) with the invertibility constraint satisfied. Then, we have the following holds with probability of at least* $1 - \delta$*:*

$$\mathbb{E}\left[\sum_{i=1}^{D}\sum_{j=1}^{D_q}\left(\partial[\widehat{\boldsymbol{f}}_{\mathrm{S}}(\boldsymbol{x}^{(q)})]_i/\partial c_j^{(q)}\right)^2\right] = O\left(\left(D\mathfrak{R}_N + \sqrt{\log(1/\delta)/N} + \nu^2\right)^{2/3}\right) \tag{8}$$

for any $\boldsymbol{c}^{(q)} \in \mathcal{C}_q$ *such that* $-C_p + \kappa_j \leq c_j^{(q)} \leq C_p - \kappa_j$ *for all* $j \in [D_q]$ *and all* $i \in [D]$*, where* $\kappa_j = \Omega((3/C_d)^{1/3}(4C_f(2D\mathfrak{R}_N + C_f\sqrt{\log(1/\delta)/2N}) + 4\nu^2)^{1/6})$*.*

The metric on the left hand side of (8) measures whether or not $\widehat{\boldsymbol{f}}_{\mathrm{S}}\left(\boldsymbol{x}^{(q)}\right)$ is a function of $\boldsymbol{c}^{(q)}$. If this metric is zero, then $\widehat{\boldsymbol{f}}_{\mathrm{S}}\left(\boldsymbol{x}^{(q)}\right)$ is disentangled from $\boldsymbol{c}^{(q)}$. The theorem indicates that with N samples, the metric is bounded by $O(N^{-1/3})$. In addition, $\mathfrak{R}_N$ decreases when N increases; e.g., a fully connected neural network with bounded weights satisfies $\mathfrak{R}_N = O(N^{-1/2})$ (Shalev-Shwartz & Ben-David, 2014). When $\mathfrak{R}_N$ increases (e.g., by using a more complex neural network), the function mismatch ν often decreases (since $\mathcal{F}$ can be more expressive with a higher $\mathfrak{R}_N$).

4 Implementation

In this section, we propose an optimization strategy to realize the criterion in (6).

Enforcing Group Statistical Independence. A notable challenge is the statistical independence constraint in (6d), whose enforcement is often an art. Early methods such as (Taleb & Jutten, 1999; Hyvärinen & Oja, 2000) may be costly. The HSIC method in (Lopez et al., 2018) that maximizes the correlation of two variables in a kernel space can be used in our framework, but kernels sometimes induce large memory overheads and are sensitive to parameter (e.g., kernel width) selection.

In this work, we provide a simple alternative. Note that if two variables X and Y are statistically independent, then we have $p(X,Y) = p(X)p(Y) \iff \mathbb{E}[\phi(X)\tau(Y)] = \mathbb{E}[\phi(X)]\mathbb{E}[\tau(Y)]$ for all measurable functions $\phi(\cdot) : \mathbb{R} \to \mathbb{R}$ and $\tau(\cdot) : \mathbb{R} \to \mathbb{R}$ (Gretton et al., 2005b). Hence, to enforce *group* independence between variables $\widehat{\boldsymbol{z}}$ and $\widehat{\boldsymbol{c}}^{(q)}$, we propose to exhaust the space of all measurable functions $\boldsymbol{\phi}^{(q)} : \mathbb{R}^D \to \mathbb{R}$ and $\boldsymbol{\tau}^{(q)} : \mathbb{R}^{D_q} \to \mathbb{R}$, such that

$$\sup_{\boldsymbol{\phi}^{(q)},\boldsymbol{\tau}^{(q)}} \mathcal{R}^{(q)} = \sup_{\boldsymbol{\phi}^{(q)},\boldsymbol{\tau}^{(q)}} \left|\mathbb{C}\mathrm{ov}\left[\boldsymbol{\phi}^{(q)}(\widehat{\boldsymbol{z}})\boldsymbol{\tau}^{(q)}(\widehat{\boldsymbol{c}}^{(q)})\right]\right| \Big/ \left(\sqrt{\mathbb{V}[\boldsymbol{\phi}^{(q)}(\widehat{\boldsymbol{z}})]}\sqrt{\mathbb{V}\left[\boldsymbol{\tau}^{(q)}(\widehat{\boldsymbol{c}}^{(q)})\right]}\right) \tag{9}$$

is minimized. It is not hard to show the following (see the proof in the supplementary material):

Proposition 1 *In (9), if $\sup_{\boldsymbol{\phi}^{(q)},\boldsymbol{\tau}^{(q)}} \mathcal{R}^{(q)} = 0$ over all measurable functions $\boldsymbol{\phi}^{(q)}$ and $\boldsymbol{\tau}^{(q)}$, then, any $[\boldsymbol{z}]_i$ and $\left[\boldsymbol{c}^{(q)}\right]_j$ for $i \in [D]$ and $j \in [D_q]$ are statistically independent.*

In practice, we use two neural networks to represent $\boldsymbol{\phi}^{(q)}$ and $\boldsymbol{\tau}^{(q)}$, respectively, which blends well with the neural encoders for algorithm design.

Reformulation and Optimization. We use deep neural networks to serve as $\boldsymbol{f}^{(q)}$. We introduce a slack variable $\boldsymbol{u}_\ell$ and change the objective to minimizing $\mathcal{L}_\ell = \sum_{q=1}^{2} \|\boldsymbol{u}_\ell - \boldsymbol{f}_{\mathrm{S}}^{(q)}(\boldsymbol{x}_\ell^{(q)})\|_2^2$ like in (3). The slack variable can also make orthogonality and zero-mean constraints easier to enforce. The invertibility constraint in (6b) can be enforced using the idea of autoencoder. Specifically, the reconstruction loss $\mathcal{V}_\ell = \sum_{q=1}^{2} \|\boldsymbol{x}_\ell^{(q)} - \boldsymbol{r}^{(q)}(\boldsymbol{f}^{(q)}(\boldsymbol{x}_\ell^{(q)}))\|_2^2$ is employed to promote invertibility of $\boldsymbol{f}^{(q)}$, where $\boldsymbol{r}^{(q)}$ is a reconstruction network. Other realizations for invertible mappings such as *flow* based methods, e.g., (Dinh et al., 2016; Kingma & Dhariwal, 2018) are also viable. Let $\boldsymbol{\theta}$ collect the parameters of $\boldsymbol{f}^{(q)}$ and $\boldsymbol{r}^{(q)}$, and $\boldsymbol{\eta}$ the parameters of $\boldsymbol{\phi}^{(q)}, \boldsymbol{\tau}^{(q)}$. The overall formulation is:

$$\min_{\boldsymbol{U},\boldsymbol{\theta}} \max_{\boldsymbol{\eta}} \ \mathcal{L} + \beta\mathcal{V} + \lambda\mathcal{R}, \quad \text{s.t.} \ \frac{1}{N}\sum_{\ell=1}^{N} \boldsymbol{u}_\ell \boldsymbol{u}_\ell^\top = \boldsymbol{I}, \ \frac{1}{N}\sum_{\ell=1}^{N} \boldsymbol{u}_\ell = \boldsymbol{0}, \tag{10}$$

where $\mathcal{L} = {}^1\!/_N \sum_{\ell=1}^{N} \mathcal{L}_\ell$, $\mathcal{V} = {}^1\!/_N \sum_{\ell=1}^{N} \mathcal{V}_\ell$, $\boldsymbol{U} = [\boldsymbol{u}_1, \cdots, \boldsymbol{u}_N] \in \mathbb{R}^{D\times N}$, $\mathcal{R} = \sum_{q=1}^{2} \mathcal{R}^{(q)}$, and $\beta, \lambda \geq 0$. See the supplementary material for our proposed algorithm for handling (10).

5 Related Work - Nonlinear ICA and Latent Disentanglement

Other than the DCCA and AM-SSL works, our design for private and shared information separation also draws insights from two topics in unsupervised representation learning, namely, nonlinear ICA (nICA) (Hyvarinen & Morioka, 2016; 2017; Hyvarinen et al., 2019; Khemakhem et al., 2020) and latent factor disentanglement (Higgins et al., 2017; Kim & Mnih, 2018; Chen et al., 2018; Zhao et al., 2019; Lopez et al., 2018), which are recently offered a unifying perspective in (Khemakhem et al., 2020). The nICA works aim to *separate* nonlinearly mixed latent components to an individual component level, which is in general impossible unless additional information associated with each sample (e.g., time frame labels (Hyvarinen & Morioka, 2016) and class labels (Hyvarinen et al., 2019; Khemakhem et al., 2020)) is used. Multiple views are less studied in the context of nICA, with the recent exception in (Locatello et al., 2020) and (Gresele et al., 2020). Nonetheless, their models are different from ours and the approaches cannot extract the private information from views with different nonlinear models. None of these works offered finite sample analysis as we did in Theorem 3, to our best knowledge. Our independence promoter is reminiscent of (Gretton et al., 2005b), with the extension to handle group variables.

6 Experiments

In this section, we provide a number of experiments to validate our theoretical results.

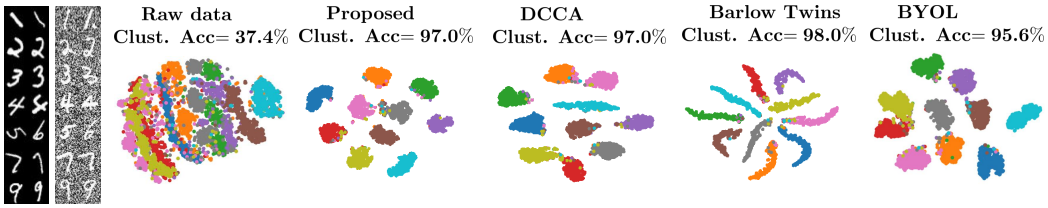

Figure 1: t-SNE of the results on multiview MNIST from (Wang et al., 2015). Baselines: `DCCA` (Wang et al., 2015), `Barlow Twins` (Zbontar et al., 2021) and `BYOL` (Grill et al., 2020) .

Synthetic Data. We first use synthetic data that are perfectly aligned with our generative model in (5) to validate our theorems. The results are relegated to the supplementary materials.

6.1 Validating Theorem 1 - Shared Component Learning

In this subsection, we show that latent correlation maximization (or latent component matching) leads to shared component extraction under the model in (5)—which can be used to explain the effectiveness of a number of DCCA and AM-SSL formulations. This is also the objective of our formulation (6) if the constraint in (6d) is not enforced.

Multiview MNIST Data. For proof-of-concept, we adopt a multiview MNIST dataset that was used in (Wang et al., 2015). There, the "augmented" view of MNIST contains randomly rotated digits and the other with additive Gaussian white noise (Wang et al., 2015); see Fig. 1. This is similar to the data augmentation ideas in AM-SSL. Using this multiview data, we apply different multiview learning paradigms that match the latent representations (or maximize the correlations of learned representations) across views. The dataset has 70,000 samples that are 28×28 images of handwritten digits. Note that without (6d), our method can be understood as a slight variant of (3). To benchmark our method, we use a number of DCCA and AM-SSL approaches mentioned in Sec. 2, namely, `DCCA` (Wang et al., 2015), `Barlow Twins` (Zbontar et al., 2021) and `BYOL` (Grill et al., 2020). We set $D = 10$, $D_1 = 20$ and $D_2 = 50$. The detailed settings of our neural networks can be found in the supplementary material.

To evaluate the effectiveness of shared information extraction, we apply k-means to all the embeddings $\widehat{\boldsymbol{z}}_\ell^{(1)} = \boldsymbol{f}_{\rm S}^{(1)}(\boldsymbol{x}_\ell^{(1)})$ and compute the clustering accuracy on the test set. In Fig. 1, we show the t-SNE (Hinton & Roweis, 2002) visualizations of $\widehat{\boldsymbol{z}}_\ell^{(1)}$'s on a test set of 10,000 samples together with the clustering accuracy. All results are averaged over 5 random initializations.

By Theorem 1, all the methods under test should output identity-revealing representations of the data samples. The reason is that the two views share the same identity information of a sample. Indeed, from Fig. 1, one can see that all latent correlation-maximization-based DCCA and AM-SSL methods learn informative representations that are sufficiently distinguishable. The "shape" of the clusters are different, which can be explained by the existence of the invertible function $\boldsymbol{\gamma}(\cdot)$. These results corroborate our analysis in Theorem 1.

CIFAR10 Data. We also observe similar results using the CIFAR10 data (Krizhevsky et al., 2009). The results can be found in the supplementary materials, due to page limitations.

6.2 Validating Theorem 2 - Shared and Private Component Disentanglement

We use data generation examples to support our claim in Theorem 2—i.e., with our designed regularizer $\mathcal{R}$ in (10), one can provably disentangle the shared and private latent components.

Cars3D Data for Cross-sample Data Generation. We use the Cars3D dataset (Reed et al., 2015) that contains different car CAD models. For each car image, there are three defining aspects (namely, 'type', 'elevation' and 'azimuth').

We create two views as follows. We assume that given the car type that is captured by shared variables $\boldsymbol{z}$ and the azimuths that are captured by $\boldsymbol{c}^{(q)}$, the generation mappings $\boldsymbol{g}^{(1)}$ and $\boldsymbol{g}^{(2)}$ produce

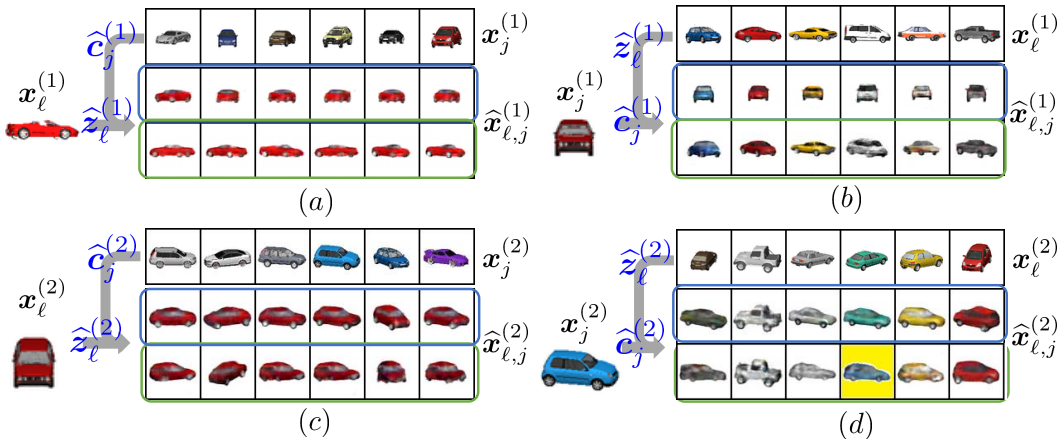

Figure 2: Evaluation on Cars3D; rows in blue boxes are w/ $\mathcal{R}$; rows in green boxes are w/o $\mathcal{R}$.

car images with low elevations and high elevations, respectively (so they must be different mappings). Under our setting, each view has $N = 8,784$ car images. We model $\boldsymbol{z}$ with $D = 10$. For $\boldsymbol{c}^{(q)}$, we set $D_1 = D_2 = 2$. More details about our settings are in the supplementary material.

We use the idea of cross-sample data generation to evaluate the effectiveness of our method. To be precise, we evaluate the learned $\widehat{\boldsymbol{f}}^{(q)}$'s by combining $\widehat{\boldsymbol{z}}_\ell^{(q)} = \widehat{\boldsymbol{f}}_{\mathrm{S}}^{(q)}(\boldsymbol{x}_\ell^{(q)})$ and $\widehat{\boldsymbol{c}}_j^{(q)} = \widehat{\boldsymbol{f}}_{\mathrm{P}}^{(q)}(\boldsymbol{x}_j^{(q)})$ and generating $\widehat{\boldsymbol{x}}_{\ell,j}^{(q)} = \widehat{\boldsymbol{r}}^{(q)}([(\widehat{\boldsymbol{z}}_\ell^{(q)})^\top, (\boldsymbol{c}_j^{(q)})^\top]^\top)$, where $\widehat{\boldsymbol{r}}^{(q)}$ is the learned reconstruction network [cf Eq. (10)]. *Under our model, if the shared components and private components are truly disentangled in the latent domain, this generated sample $\widehat{\boldsymbol{x}}_{\ell,j}^{(q)}$ should exhibit the same 'type' and 'elevation' as those of $\boldsymbol{x}_\ell^{(q)}$ and the 'azimuth' of $\boldsymbol{x}_j^{(q)}$.*

Fig. 2 shows our experiment results. The proposed method's outputs are as expected. For example, in subfigure (a), the $\boldsymbol{z}_\ell^{(1)}$ is extracted from the red convertible, and the $\widehat{\boldsymbol{c}}_j^{(1)}$'s are extracted from the top row. One can see that the generated $\widehat{\boldsymbol{x}}_{\ell,j}^{(1)}$'s under the proposed method with $\mathcal{R}$ are all red convertibles with the same elevation, but using the azimuths of the corresponding cars from the top row. Note that if $\mathcal{R}$ is not used, then the learned $\widehat{\boldsymbol{c}}_j^{(q)}$ may still contain the 'type' or 'elevation' information; see the example highlighted with yellow background in subfigure (d). More results are in the supplementary material.

dSprites Data and MNIST Data for Cross-sample/Cross-view Data Generation. We offer two extra sets of examples to validate our claim in Theorem 2. Please see the supplementary materials.

7 Conclusion

In this work, we provided theoretical understandings to the effectiveness of latent correlation maximization (latent component matching) based DCCA and AM-SSL methods from an unsupervised nonlinear mixture learning viewpoint. In particular, we modeled multiview data as nonlinear mixtures of shared and private components, and showed that latent correlation maximization ensures to extract the shared components—which are believed to be identity-revealing. In addition, we showed that, with a carefully designed constraint (which is later realized by a neural regularizer), one can further disentangle the shared and private information, under reasonable conditions. We also analyzed the sample complexity for extracting the shared information, which has not been addressed in nonlinear component analysis works, to our best knowledge. To realize our learning criterion, we proposed a slack variable-assisted latent correlation maximization approach, with a novel minimax neural regularizer for promoting group independence. We tested our method over synthetic and real data. The results corroborated our design goals and theoretical analyses.

Ethics Statement. This paper focuses on theoretical analysis and provable guarantees of learning criteria. It does not involve human subjects or other ethics-related concerns.

Reproducibility Statement. The authors strive to make the research in this work reproducible. The supplementary materials contain rich details of the algorithm implementation and experiment settings. The source code of our Python-implemented algorithm and two demos with real data are uploaded as supplementary materials. The details of the proofs of our theoretical claims are also included in the supplementary materials.

REFERENCES

Galen Andrew, Raman Arora, Jeff Bilmes, and Karen Livescu. Deep canonical correlation analysis. In *International Conference on Machine Learning*, pp. 1247–1255. PMLR, 2013.

Francis R Bach and Michael I Jordan. A probabilistic interpretation of canonical correlation analysis. 2005.

Peter L Bartlett and Shahar Mendelson. Rademacher and Gaussian complexities: Risk bounds and structural results. *Journal of Machine Learning Research*, 3(Nov):463–482, 2002.

Mohamed Ishmael Belghazi, Aristide Baratin, Sai Rajeshwar, Sherjil Ozair, Yoshua Bengio, Aaron Courville, and Devon Hjelm. MINE: Mutual information neural estimation. In *International Conference on Machine Learning*, volume 80, pp. 531–540. PMLR, 10–15 Jul 2018.

Adrian Benton, Huda Khayrallah, Biman Gujral, Drew Reisinger, Shenmin Zhang, and Raman Arora. Deep generalized canonical correlation analysis. In *RepL4NLP at ACL*, 2017.

J Douglas Carroll. Generalization of canonical correlation analysis to three or more sets of variables. In *Proceedings of the 76th annual convention of the American Psychological Association*, volume 3, pp. 227–228, 1968.

Ricky TQ Chen, Xuechen Li, Roger B Grosse, and David K Duvenaud. Isolating sources of disentanglement in variational autoencoders. In *Advances in Neural Information Processing Systems*, pp. 2610–2620, 2018.

Ting Chen, Simon Kornblith, Mohammad Norouzi, and Geoffrey Hinton. A simple framework for contrastive learning of visual representations. In *International Conference on Machine Learning*, pp. 1597–1607. PMLR, 2020.

Xinlei Chen and Kaiming He. Exploring simple Siamese representation learning. In *Proceedings of Conference on Computer Vision and Pattern Recognition*, pp. 15750–15758, 2021.

Richard A Davis, Keh-Shin Lii, and Dimitris N Politis. Remarks on some nonparametric estimates of a density function. In *Selected Works of Murray Rosenblatt*, pp. 95–100. Springer, 2011.

Laurent Dinh, Jascha Sohl-Dickstein, and Samy Bengio. Density estimation using real nvp. *arXiv preprint arXiv:1605.08803*, 2016.

Alexey Dosovitskiy, Philipp Fischer, Jost Tobias Springenberg, Martin Riedmiller, and Thomas Brox. Discriminative unsupervised feature learning with exemplar convolutional neural networks. *IEEE Trans. Pattern Anal. Mach. Intell.*, 38(9):1734–1747, 2015.

John Duchi, Elad Hazan, and Yoram Singer. Adaptive subgradient methods for online learning and stochastic optimization. *Journal of Machine Learning Research*, 12(Jul):2121–2159, 2011.

Ronald A Fisher. Frequency distribution of the values of the correlation coefficient in samples from an indefinitely large population. *Biometrika*, 10(4):507–521, 1915.

Spyros Gidaris, Praveer Singh, and Nikos Komodakis. Unsupervised representation learning by predicting image rotations. In *International Conference on Learning Representations*, 2018.

Luigi Gresele, Paul K Rubenstein, Arash Mehrjou, Francesco Locatello, and Bernhard Schölkopf. The incomplete Rosetta stone problem: Identifiability results for multi-view nonlinear ICA. In *Proceedings of UAI 2020*, pp. 217–227, 2020.

Arthur Gretton, Olivier Bousquet, Alex Smola, and Bernhard Schölkopf. Measuring statistical dependence with hilbert-schmidt norms. In *International Conference on Algorithmic Learning Theory*, pp. 63–77. Springer, 2005a.

Arthur Gretton, Alexander J Smola, Olivier Bousquet, Ralf Herbrich, Andrei Belitski, Mark Augath, Yusuke Murayama, Jon Pauls, Bernhard Schölkopf, and Nikos K Logothetis. Kernel constrained covariance for dependence measurement. In *International Conference on Artificial Intelligence and Statistics*, volume 10, pp. 112–119. Citeseer, 2005b.

Jean-Bastien Grill, Florian Strub, Florent Altché, Corentin Tallec, Pierre Richemond, Elena Buchatskaya, Carl Doersch, Bernardo Avila Pires, Zhaohan Guo, Mohammad Gheshlaghi Azar, Bilal Piot, Koray Kavukcuoglu, Remi Munos, and Michal Valko. Bootstrap your own latent - a new approach to self-supervised learning. In *Advances in Neural Information Processing Systems*, volume 33, pp. 21271–21284, 2020.

Gregory Gundersen, Bianca Dumitrascu, Jordan T Ash, and Barbara E Engelhardt. End-to-end training of deep probabilistic cca on paired biomedical observations. In *Uncertainty in artificial intelligence*, 2019.

Irina Higgins, Loic Matthey, Arka Pal, Christopher Burgess, Xavier Glorot, Matthew Botvinick, Shakir Mohamed, and Alexander Lerchner. Beta-VAE: Learning basic visual concepts with a constrained variational framework. In *International Conference on Learning Representations*, 2017.

Geoffrey Hinton and Sam T Roweis. Stochastic neighbor embedding. In *Advances in Neural Information Processing Systems*, volume 15, pp. 833–840, 2002.

Harold Hotelling. Relations between two sets of variates. *Biometrika*, 28(3/4):321–377, 1936.

Xun Huang, Ming-Yu Liu, Serge Belongie, and Jan Kautz. Multimodal unsupervised image-to-image translation. In *Proceedings of the European Conference on Computer Vision*, pp. 172–189, 2018.

Aapo Hyvarinen and Hiroshi Morioka. Unsupervised feature extraction by time-contrastive learning and nonlinear ica. In *Advances in Neural Information Processing Systems*, volume 29, 2016.

Aapo Hyvarinen and Hiroshi Morioka. Nonlinear ICA of temporally dependent stationary sources. In *International Conference on Artificial Intelligence and Statistics*, volume 54, pp. 460–469, 20–22 Apr 2017.

Aapo Hyvärinen and Erkki Oja. Independent component analysis: Algorithms and applications. *Neural Networks*, 13(4-5):411–430, 2000.

Aapo Hyvarinen, Hiroaki Sasaki, and Richard Turner. Nonlinear ICA using auxiliary variables and generalized contrastive learning. In *International Conference on Artificial Intelligence and Statistics*, pp. 859–868, 2019.

Mohamed Salah Ibrahim and Nicholas D Sidiropoulos. Reliable detection of unknown cell-edge users via canonical correlation analysis. *IEEE Trans. Wireless Commun.*, 19(6):4170–4182, 2020.

Jon R Kettenring. Canonical analysis of several sets of variables. *Biometrika*, 58(3):433–451, 1971.

Ilyes Khemakhem, Diederik Kingma, Ricardo Monti, and Aapo Hyvarinen. Variational autoencoders and nonlinear ICA: A unifying framework. In *International Conference on Artificial Intelligence and Statistics*, pp. 2207–2217. PMLR, 2020.

Hyunjik Kim and Andriy Mnih. Disentangling by factorising. In *International Conference on Machine Learning*, volume 80, pp. 2649–2658. PMLR, 10–15 Jul 2018.

Diederik P Kingma and Jimmy Ba. Adam: A method for stochastic optimization. *arXiv preprint arXiv:1412.6980*, 2014.

Diederik P Kingma and Prafulla Dhariwal. Glow: Generative flow with invertible 1x1 convolutions. *arXiv preprint arXiv:1807.03039*, 2018.

Alex Krizhevsky, Geoffrey Hinton, et al. Learning multiple layers of features from tiny images. 2009.

Pei Ling Lai and Colin Fyfe. Kernel and nonlinear canonical correlation analysis. *International Journal of Neural Systems*, 10(05):365–377, 2000.

Hsin-Ying Lee, Hung-Yu Tseng, Jia-Bin Huang, Maneesh Singh, and Ming-Hsuan Yang. Diverse image-to-image translation via disentangled representations. In *Proceedings of the European Conference on Computer Vision*, pp. 35–51, 2018.

Francesco Locatello, Ben Poole, Gunnar Rätsch, Bernhard Schölkopf, Olivier Bachem, and Michael Tschannen. Weakly-supervised disentanglement without compromises. In *International Conference on Machine Learning*, pp. 6348–6359. PMLR, 2020.

Romain Lopez, Jeffrey Regier, Michael I Jordan, and Nir Yosef. Information constraints on auto-encoding variational Bayes. *Advances in Neural Information Processing Systems*, 31:6114–6125, 2018.

Qi Lyu and Xiao Fu. Nonlinear multiview analysis: Identifiability and neural network-assisted implementation. *IEEE Trans. Signal Process.*, 68:2697–2712, 2020.

Mehryar Mohri, Afshin Rostamizadeh, and Ameet Talwalkar. *Foundations of Machine Learning*. MIT press, 2018.

Pushpendre Rastogi, Benjamin Van Durme, and Raman Arora. Multiview LSA: Representation learning via generalized CCA. In *Proceedings of the 2015 conference of the North American chapter of the Association for Computational Linguistics: Human Language Technologies*, pp. 556–566, 2015.

Scott E Reed, Yi Zhang, Yuting Zhang, and Honglak Lee. Deep visual analogy-making. *Advances in Neural Information Processing Systems*, 28:1252–1260, 2015.

Shai Shalev-Shwartz and Shai Ben-David. *Understanding machine learning: From theory to algorithms*. Cambridge university press, 2014.

Anisse Taleb and Christian Jutten. Source separation in post-nonlinear mixtures. *IEEE Trans. Signal Process.*, 47(10):2807–2820, 1999.

Julius von Kügelgen, Yash Sharma, Luigi Gresele, Wieland Brendel, Bernhard Schölkopf, Michel Besserve, and Francesco Locatello. Self-supervised learning with data augmentations provably isolates content from style. *arXiv preprint arXiv:2106.04619*, 2021.

Weiran Wang, Raman Arora, Karen Livescu, and Jeff Bilmes. On deep multi-view representation learning. In *International Conference on Machine Learning*, pp. 1083–1092, 2015.

Weiran Wang, Xinchen Yan, Honglak Lee, and Karen Livescu. Deep variational canonical correlation analysis. *arXiv preprint arXiv:1610.03454*, 2016.

Ka Yee Yeung and Walter L Ruzzo. Details of the Adjusted Rand Index and clustering algorithms, supplement to the paper an empirical study on Principal Component Analysis for clustering gene expression data. *Bioinformatics*, 17(9):763–774, 2001.

Jure Zbontar, Li Jing, Ishan Misra, Yann Lecun, and Stephane Deny. Barlow Twins: Self-supervised learning via redundancy reduction. In *Proceedings of the 38th International Conference on Machine Learning*, volume 139 of *Proceedings of Machine Learning Research*, pp. 12310–12320. PMLR, 18–24 Jul 2021.

Shengjia Zhao, Jiaming Song, and Stefano Ermon. InfoVAE: Balancing learning and inference in variational autoencoders. *Proceedings of the AAAI Conference on Artificial Intelligence*, 33(01): 5885–5892, Jul. 2019.

Supplementary Materials

A NOTATION

The notations used in this work are summarized in Table A.1.

Table A.1: Definition of notations.

Notation	Definition
$x, \boldsymbol{x}, \boldsymbol{X}$	scalar, vector, and matrix
$[\boldsymbol{x}]_i, x_i$	both represent the ith element of vector $\boldsymbol{x}$
$[\boldsymbol{X}]_{ij}$	the ith row, jth column of matrix $\boldsymbol{X}$
$p(\boldsymbol{x})$	probability density function of random variable $\boldsymbol{x}$
$x \perp\!\!\!\perp y$	x and y are statistically independent, i.e., $p(x,y) = p(x)p(y)$
$\boldsymbol{x} \perp\!\!\!\perp \boldsymbol{y}$	$x_i \perp\!\!\!\perp y_j$ for all i, j
$\boldsymbol{x}^\top, \boldsymbol{X}^\top$	transpose of $\boldsymbol{x}$, $\boldsymbol{X}$
$\boldsymbol{J}_{\boldsymbol{f}}$	Jocobian matrix of a vector-valued function $\boldsymbol{f}$
$\boldsymbol{I}$	identity matrix with a proper size
$\boldsymbol{f} \circ \boldsymbol{g}$	function composition operation
$\det \boldsymbol{X}$	determinant of a square matrix $\boldsymbol{X}$
$\mathbb{E}[\cdot]$	expectation
$\mathbb{V}[\cdot]$	variance
$\mathbb{C}\mathbb{o}\mathbb{v}[\cdot,\cdot]$	covariance
$[N]$	the integer set $\{1, 2, \ldots, N\}$

B PROOF OF THEOREM 1

Theorem 1. (**Shared Component Extraction**) Under the generative model in (5) and Assumption 1, consider the population form in (6) (i.e., $N = \infty$). Assume that the considered constraints hold over all $\boldsymbol{x}^{(q)} \in \mathcal{X}_q$ for $q = 1, 2$, where $\mathcal{X}_q = \{\boldsymbol{x}^{(q)} | \boldsymbol{x}^{(q)} = \boldsymbol{g}^{(q)}([\boldsymbol{z}^\top, (\boldsymbol{c}^{(q)})^\top]^\top), \forall \boldsymbol{z} \in \mathcal{Z}, \forall \boldsymbol{c}^{(q)} \in \mathcal{C}_q\}$. Denote $\widehat{\boldsymbol{f}}^{(q)}$ as *any* solution of (6). Also assume that the first-order derivative of $\widehat{\boldsymbol{f}}^{(q)} \circ \boldsymbol{g}^{(q)}$ exists. Then, we have $\widehat{\boldsymbol{z}} = \widehat{\boldsymbol{f}}_{\mathrm{S}}^{(q)}\left(\boldsymbol{x}^{(q)}\right) = \boldsymbol{\gamma}(\boldsymbol{z})$ no matter if (6d) is enforced or not, where $\boldsymbol{\gamma}(\cdot) : \mathbb{R}^D \to \mathbb{R}^D$ is a certain invertible functions.

We consider the formulation in (6) *without* (6d). When $N = \infty$ and $\boldsymbol{x}^{(q)} \sim \mathcal{X}_q$ for $q = 1, 2$ are all available, the sample average version of the formulation in (6) becomes the following expected value version:

$$\underset{\boldsymbol{f}^{(1)}, \boldsymbol{f}^{(2)}}{\text{maximize}} \ \mathrm{Tr}\left(\mathbb{E}\left[\boldsymbol{f}_{\mathrm{S}}^{(1)}\left(\boldsymbol{x}_\ell^{(1)}\right)\left(\boldsymbol{f}_{\mathrm{S}}^{(2)}\left(\boldsymbol{x}_\ell^{(2)}\right)\right)^\top\right]\right) \tag{B.1a}$$

$$\text{subject to } \boldsymbol{f}^{(q)} \text{ for } q = 1, 2 \text{ are invertible,} \tag{B.1b}$$

$$\mathbb{E}\left[\boldsymbol{f}_{\mathrm{S}}^{(q)}\left(\boldsymbol{x}_\ell^{(q)}\right)\boldsymbol{f}_{\mathrm{S}}^{(q)}\left(\boldsymbol{x}_\ell^{(q)}\right)^\top\right] = \boldsymbol{I}, \ \mathbb{E}\left[\boldsymbol{f}_{\mathrm{S}}\left(\boldsymbol{x}_\ell^{(q)}\right)\right] = \boldsymbol{0}, \ q = 1, 2 \tag{B.1c}$$

First, note that under the generative model in (5), the maximum of the objective function in (6) is D, which is obtained when every corresponding components of the learned solutions, i.e., $\widehat{\boldsymbol{f}}_{\mathrm{S}}^{(1)} : \mathbb{R}^{M_1} \to \mathbb{R}^D$ and $\widehat{\boldsymbol{f}}_{\mathrm{S}}^{(1)} : \mathbb{R}^{M_2} \to \mathbb{R}^D$, are perfectly correlated, i.e.,

$$\widehat{\boldsymbol{f}}_{\mathrm{S}}^{(1)}\left(\boldsymbol{x}^{(1)}\right) = \widehat{\boldsymbol{f}}_{\mathrm{S}}^{(2)}\left(\boldsymbol{x}^{(2)}\right). \tag{B.2}$$

Indeed, one may rewrite (B.1a) as

$$\begin{aligned}
&\arg\min_{\boldsymbol{f}^{(1)},\boldsymbol{f}^{(2)}} \; -2\mathrm{Tr}\left(\mathbb{E}\left[\boldsymbol{f}_{\mathrm{S}}^{(1)}\left(\boldsymbol{x}_{\ell}^{(1)}\right)\left(\boldsymbol{f}_{\mathrm{S}}^{(2)}\left(\boldsymbol{x}_{\ell}^{(2)}\right)^{\top}\right)\right]\right) \\
=&\arg\min_{\boldsymbol{f}^{(1)},\boldsymbol{f}^{(2)}} \; \boldsymbol{I}-2\mathrm{Tr}\left(\mathbb{E}\left[\boldsymbol{f}_{\mathrm{S}}^{(1)}\left(\boldsymbol{x}_{\ell}^{(1)}\right)\left(\boldsymbol{f}_{\mathrm{S}}^{(2)}\left(\boldsymbol{x}_{\ell}^{(2)}\right)^{\top}\right)\right]\right)+\boldsymbol{I} \\
=&\arg\min_{\boldsymbol{f}^{(1)},\boldsymbol{f}^{(2)}} \; \mathbb{E}\left[\left\|\boldsymbol{f}_{\mathrm{S}}^{(1)}\left(\boldsymbol{x}_{\ell}^{(1)}\right)-\boldsymbol{f}_{\mathrm{S}}^{(2)}\left(\boldsymbol{x}_{\ell}^{(2)}\right)\right\|_2^2\right]
\end{aligned} \tag{B.3}$$

where the second equality holds because the constraint in (B.1c). Note that the criterion in (B.3) admits the optimal solution in (B.2) under our generative model.

Note that one solution to attain zero cost of (B.3) is

$$\widehat{\boldsymbol{f}}_{\mathrm{S}}^{(q)}\left(\boldsymbol{x}^{(q)}\right)=\boldsymbol{z},\; q=1,2.$$

However, the question lies in "uniqueness", i.e., can enforcing (B.2) always yield $\boldsymbol{f}_{\mathrm{S}}^{(q)}\left(\boldsymbol{x}^{(q)}\right)=\boldsymbol{z}$ (up to certain ambiguities)? This is central to learning criterion design, as the expressiveness of function approximators like neural networks may attain zero cost of (B.3) with undesired solutions.

Assume that a solution that satisfies (B.2) is found. Denote $\widehat{\boldsymbol{f}}^{(q)}$ for $q=1,2$ as the solution. Combine the solution with the generative model in (5). Then, following equality can be obtained:

$$\boldsymbol{h}_{\mathrm{S}}^{(1)}\left(\begin{bmatrix}\boldsymbol{z}\\ \boldsymbol{c}^{(1)}\end{bmatrix}\right)=\boldsymbol{h}_{\mathrm{S}}^{(2)}\left(\begin{bmatrix}\boldsymbol{z}\\ \boldsymbol{c}^{(2)}\end{bmatrix}\right), \tag{B.4}$$

where we have

$$\boldsymbol{h}_{\mathrm{S}}^{(q)}(\boldsymbol{\omega}^{(q)})=\left[\widehat{\boldsymbol{f}}^{(q)}\circ\boldsymbol{g}^{(q)}\left(\boldsymbol{\omega}^{(q)}\right)\right]_{1:D}=\widehat{\boldsymbol{f}}_{\mathrm{S}}^{(q)}\circ\boldsymbol{g}^{(q)}\left(\boldsymbol{\omega}^{(q)}\right),$$

in which

$$\boldsymbol{\omega}^{(q)}=[\boldsymbol{z}^{\top},(\boldsymbol{c}^{(q)})^{\top}]^{\top}.$$

We hope to show that $\boldsymbol{h}_{\mathrm{S}}^{(1)}$ and $\boldsymbol{h}_{\mathrm{S}}^{(2)}$ are functions of only $\boldsymbol{z}$—i.e., the functions $\widehat{\boldsymbol{f}}_{\mathrm{S}}^{(q)}$ for $q=1,2$ only extract the shared information.

To show that $\boldsymbol{h}_{\mathrm{S}}^{(1)}$ is a function of only $\boldsymbol{z}$ but not a function of $\boldsymbol{c}^{(1)}$, we consider the first-order partial derivatives of $\boldsymbol{h}_{\mathrm{S}}^{(1)}$ w.r.t. $\boldsymbol{z}$ and $\boldsymbol{c}^{(1)}$, respectively. Namely, we hope to show that the matrix consisting of all the partial derivatives of $\boldsymbol{h}_{\mathrm{S}}^{(1)}$ w.r.t. $\boldsymbol{z}$ is full rank while any partial derivatives of $\boldsymbol{h}_{\mathrm{S}}^{(1)}$ w.r.t. $\boldsymbol{z}$ is zero.

Therefore, we investigate the Jacobian of $\boldsymbol{h}^{(1)}$ which fully characterizes all the first-order partial derivatives of the function $\boldsymbol{h}_{\mathrm{S}}^{(1)}$ and $\boldsymbol{h}_{\mathrm{P}}^{(1)}$ w.r.t. $\boldsymbol{z}$ and $\boldsymbol{c}^{(1)}$. Let us denote the outputs of $\boldsymbol{h}^{(1)}=\widehat{\boldsymbol{f}}^{(1)}\circ\boldsymbol{g}^{(1)}(\boldsymbol{\omega}^{(1)})$ as follows:

$$\begin{bmatrix}\widehat{\boldsymbol{z}}\\ \widehat{\boldsymbol{c}}^{(1)}\end{bmatrix}=\boldsymbol{h}^{(1)}\left(\begin{bmatrix}\boldsymbol{z}\\ \boldsymbol{c}^{(1)}\end{bmatrix}\right). \tag{B.5}$$

The Jacobian of $\boldsymbol{h}^{(1)}$ can be expressed using the following block form

$$\boldsymbol{J}^{(1)}=\begin{bmatrix}\boldsymbol{J}_{11}^{(1)} & \boldsymbol{J}_{12}^{(1)}\\ \boldsymbol{J}_{21}^{(1)} & \boldsymbol{J}_{22}^{(1)}\end{bmatrix},$$

where $\boldsymbol{J}_{11}^{(1)} \in \mathbb{R}^{D\times D}$, $\boldsymbol{J}_{12}^{(1)} \in \mathbb{R}^{D\times D_1}$, $\boldsymbol{J}_{21}^{(1)} \in \mathbb{R}^{D_1\times D}$ and $\boldsymbol{J}_{22}^{(1)} \in \mathbb{R}^{D_1\times D_1}$ are Jacobian matrices defined as follows

$$\boldsymbol{J}_{11}^{(1)} = \begin{bmatrix} \frac{\partial\left[\boldsymbol{h}_{\mathrm{S}}^{(1)}(\boldsymbol{\omega}^{(1)})\right]_1}{\partial z_1} & \cdots & \frac{\partial\left[\boldsymbol{h}_{\mathrm{S}}^{(1)}(\boldsymbol{\omega}^{(1)})\right]_1}{\partial z_D} \\ \vdots & \ddots & \vdots \\ \frac{\partial\left[\boldsymbol{h}_{\mathrm{S}}^{(1)}(\boldsymbol{\omega}^{(1)})\right]_D}{\partial z_1} & \cdots & \frac{\partial\left[\boldsymbol{h}_{\mathrm{S}}^{(1)}(\boldsymbol{\omega}^{(1)})\right]_D}{\partial z_D} \end{bmatrix}, \boldsymbol{J}_{12}^{(1)} = \begin{bmatrix} \frac{\partial\left[\boldsymbol{h}_{\mathrm{S}}^{(1)}(\boldsymbol{\omega}^{(1)})\right]_1}{\partial c_1^{(1)}} & \cdots & \frac{\partial\left[\boldsymbol{h}_{\mathrm{S}}^{(1)}(\boldsymbol{\omega}^{(1)})\right]_1}{\partial c_{D_1}^{(1)}} \\ \vdots & \ddots & \vdots \\ \frac{\partial\left[\boldsymbol{h}_{\mathrm{S}}^{(1)}(\boldsymbol{\omega}^{(1)})\right]_D}{\partial c_1^{(1)}} & \cdots & \frac{\partial\left[\boldsymbol{h}_{\mathrm{S}}^{(1)}(\boldsymbol{\omega}^{(1)})\right]_D}{\partial c_{D_1}^{(1)}} \end{bmatrix},$$

$$\boldsymbol{J}_{21}^{(1)} = \begin{bmatrix} \frac{\partial\left[\boldsymbol{h}_{\mathrm{P}}^{(1)}(\boldsymbol{\omega}^{(1)})\right]_1}{\partial z_1} & \cdots & \frac{\partial\left[\boldsymbol{h}_{\mathrm{P}}^{(1)}(\boldsymbol{\omega}^{(1)})\right]_1}{\partial z_D} \\ \vdots & \ddots & \vdots \\ \frac{\partial\left[\boldsymbol{h}_{\mathrm{P}}^{(1)}(\boldsymbol{\omega}^{(1)})\right]_{D_1}}{\partial z_1} & \cdots & \frac{\partial\left[\boldsymbol{h}_{\mathrm{P}}^{(1)}(\boldsymbol{\omega}^{(1)})\right]_{D_1}}{\partial z_D} \end{bmatrix}, \boldsymbol{J}_{22}^{(1)} = \begin{bmatrix} \frac{\partial\left[\boldsymbol{h}_{\mathrm{P}}^{(1)}(\boldsymbol{\omega}^{(1)})\right]_1}{\partial c_1^{(1)}} & \cdots & \frac{\partial\left[\boldsymbol{h}_{\mathrm{P}}^{(1)}(\boldsymbol{\omega}^{(1)})\right]_1}{\partial c_{D_1}^{(1)}} \\ \vdots & \ddots & \vdots \\ \frac{\partial\left[\boldsymbol{h}_{\mathrm{P}}^{(1)}(\boldsymbol{\omega}^{(1)})\right]_{D_1}}{\partial c_1^{(1)}} & \cdots & \frac{\partial\left[\boldsymbol{h}_{\mathrm{P}}^{(1)}(\boldsymbol{\omega}^{(1)})\right]_{D_1}}{\partial c_{D_1}^{(1)}} \end{bmatrix}.$$

What we hope to show is that $\boldsymbol{J}_{12}^{(1)}$ **is an all-zero matrix while the determinant of** $\boldsymbol{J}_{11}^{(1)}$ **is non-zero**.

We first show that $\boldsymbol{J}_{12}^{(1)} = \boldsymbol{0}$. Note that (B.4) holds over the entire domain. Hence, we consider any fixed $\overline{\boldsymbol{z}}$ and $\overline{\boldsymbol{c}}^{(2)}$. Then for all $\boldsymbol{c}^{(1)}$, the following equation holds:

$$\boldsymbol{h}_{\mathrm{S}}^{(1)}\left(\begin{bmatrix}\overline{\boldsymbol{z}} \\ \boldsymbol{c}^{(1)}\end{bmatrix}\right) = \boldsymbol{h}_{\mathrm{S}}^{(2)}\left(\begin{bmatrix}\overline{\boldsymbol{z}} \\ \overline{\boldsymbol{c}}^{(2)}\end{bmatrix}\right) \tag{B.6}$$

for all $\boldsymbol{c}^{(1)} \in \mathcal{C}_1$ with any fixed $\overline{\boldsymbol{z}}$ and $\overline{\boldsymbol{c}}^{(2)}$.

Let us define matrices $\boldsymbol{H}_{\mathrm{S}}^{(1)}$ and $\boldsymbol{H}_{\mathrm{S}}^{(2)}$, where

$$\left[\boldsymbol{H}_{\mathrm{S}}^{(q)}\right]_{i,j} = \frac{\partial\left[\boldsymbol{h}_{\mathrm{S}}^{(q)}\left(\boldsymbol{\omega}^{(q)}\right)\right]_i}{\partial c_j^{(1)}},\ i = 1, \cdots, D,\ j = 1, \cdots, D_1.$$

By taking partial derivatives of Eq. (B.6) w.r.t. $c_j^{(1)}$ for $j = 1, \ldots, D_1$, we have the following Jacobian:

$$\boldsymbol{H}_{\mathrm{S}}^{(1)}\Big|_{\overline{\boldsymbol{z}},\boldsymbol{c}^{(1)}} = \boldsymbol{H}_{\mathrm{S}}^{(2)}\Big|_{\overline{\boldsymbol{z}},\overline{\boldsymbol{c}}^{(2)}} \overset{(a)}{=} \left(\boldsymbol{J}_{\boldsymbol{h}_{\mathrm{S}}^{(2)}}\Big|_{\overline{\boldsymbol{z}},\overline{\boldsymbol{c}}^{(2)}}\right) \begin{bmatrix} \frac{\partial \overline{z}_1}{\partial c_1^{(1)}} & \cdots & \frac{\partial \overline{z}_1}{\partial c_{D_1}^{(1)}} \\ \vdots & \ddots & \vdots \\ \frac{\partial \overline{z}_D}{\partial c_1^{(1)}} & \cdots & \frac{\partial \overline{z}_D}{\partial c_{D_1}^{(1)}} \\ \frac{\partial \overline{c}_1^{(2)}}{\partial c_1^{(1)}} & \cdots & \frac{\partial \overline{c}_1^{(2)}}{\partial c_{D_1}^{(1)}} \\ \vdots & \ddots & \vdots \\ \frac{\partial \overline{c}_{D_2}^{(2)}}{\partial c_1^{(1)}} & \cdots & \frac{\partial \overline{c}_{D_2}^{(2)}}{\partial c_{D_1}^{(1)}} \end{bmatrix} \overset{(b)}{=} \left(\boldsymbol{J}_{\boldsymbol{h}_{\mathrm{S}}^{(2)}}\Big|_{\overline{\boldsymbol{z}},\overline{\boldsymbol{c}}^{(2)}}\right) \begin{bmatrix} \boldsymbol{0}_{D\times D_1} \\ \boldsymbol{0}_{D_2\times D_1} \end{bmatrix} = \boldsymbol{0}_{D\times D_1}, \tag{B.7}$$

where $\boldsymbol{J}_{\boldsymbol{h}_{\mathrm{S}}^{(2)}} \in \mathbb{R}^{D\times(D+D_2)}$ is the Jacobian of $\boldsymbol{h}_{\mathrm{S}}^{(2)}$, (a) is by the chain rules and (b) is because we take derivatives of constants. The equation above holds for any $\overline{\boldsymbol{z}}$ and $\overline{\boldsymbol{c}}^{(2)}$. Hence, the same derivation holds for all $\boldsymbol{z}$ and $\boldsymbol{c}^{(2)}$, which leads to the conclusion that the learned $\boldsymbol{h}_{\mathrm{S}}^{(q)}(\boldsymbol{\omega}^{(q)})$ is not a function of $\boldsymbol{c}^{(1)}$. Note that another possibility that could lead to (B.7) is that $\boldsymbol{h}_{\mathrm{S}}^{(q)}(\boldsymbol{\omega}^{(q)})$ always outputs a constant. However, this is not possible because each $\boldsymbol{h}^{(q)} = \widehat{\boldsymbol{f}}^{(q)} \circ \boldsymbol{g}^{(q)}$ is an invertible function, which implies that any dimension of $\boldsymbol{h}^{(q)}(\boldsymbol{\omega}^{(q)})$ cannot be a constant if $\boldsymbol{\omega}^{(q)}$ is not a constant. To be more precise, note that $\boldsymbol{x}^{(q)}$ is generated from $\boldsymbol{\omega}^{(q)}$ that has $D + D_q$ dimensions. If there are D dimensions (i.e., $\boldsymbol{h}_{\mathrm{S}}^{(q)}(\boldsymbol{\omega}^{(q)}) \in \mathbb{R}^D$) that are constants (and thus no information) in the learned generative domain, then $\boldsymbol{x}^{(q)}$ cannot be reconstructed from that domain, which contradicts invertibility.

Then, the Jacobian of $\boldsymbol{h}^{(1)}$ can be re-expressed by (B.7)

$$\boldsymbol{J}^{(1)} = \begin{bmatrix} \boldsymbol{J}_{11}^{(1)} & \boldsymbol{H}_S^{(1)} \\ \boldsymbol{J}_{21}^{(1)} & \boldsymbol{J}_{22}^{(1)} \end{bmatrix} = \begin{bmatrix} \boldsymbol{J}_{11}^{(1)} & \boldsymbol{0}_{D\times D_1} \\ \boldsymbol{J}_{21}^{(1)} & \boldsymbol{J}_{22}^{(1)} \end{bmatrix}.$$

Next, we show that the determinant of $\boldsymbol{J}_{11}^{(1)}$ is non-zero. By the structure of the Jacobian $\boldsymbol{J}^{(1)}$, one can see that $\widehat{\boldsymbol{z}}$ is a function of only $\boldsymbol{z}$ but not determined by $\boldsymbol{c}^{(1)}$, where we denote as $\widehat{\boldsymbol{z}} = \boldsymbol{\gamma}(\boldsymbol{z})$. Besides, since $\boldsymbol{h}^{(1)}$ is invertible, we have

$$\left|\det \boldsymbol{J}^{(1)}\right| = \left|\det \boldsymbol{J}_{11}^{(1)}\right| \left|\det \boldsymbol{J}_{22}^{(1)}\right| \neq 0$$

by the property of determinant for block matrix. It further indicates that $\left|\det \boldsymbol{J}_{11}^{(1)}\right| \neq 0$ (so does $\left|\det \boldsymbol{J}_{22}^{(1)}\right|$), which implies that $\boldsymbol{\gamma}(\cdot)$ is an invertible function. This proves Theorem 1. □

C Proof Of Theorem 2

Theorem 2. (**Private Component Extraction**) Under the same conditions as in Theorem 1, also assume that (6d) is enforced, we further have $\widehat{\boldsymbol{c}}^{(q)} = \widehat{\boldsymbol{f}}_{\mathrm{P}}^{(q)}\left(\boldsymbol{x}^{(q)}\right) = \boldsymbol{\delta}^{(q)}\left(\boldsymbol{c}^{(q)}\right)$, where $\boldsymbol{\delta}^{(q)}(\cdot) : \mathbb{R}^{D_q} \to \mathbb{R}^{D_q}$ is a certain invertible function.

Following the proof of Theorem 1, we further consider the expected value version with (6d), i.e.,

$$\underset{\boldsymbol{f}^{(1)},\boldsymbol{f}^{(2)}}{\text{maximize}} \ \mathrm{Tr}\left(\mathbb{E}\left[\boldsymbol{f}_{\mathrm{S}}^{(1)}\left(\boldsymbol{x}^{(1)}\right)\boldsymbol{f}_{\mathrm{S}}^{(2)}\left(\boldsymbol{x}^{(2)}\right)^{\top}\right]\right) \tag{C.1a}$$

$$\text{subject to } \boldsymbol{f}^{(q)} \text{ for } q=1,2 \text{ are invertible,} \tag{C.1b}$$

$$\mathbb{E}\left[\boldsymbol{f}_{\mathrm{S}}^{(q)}\left(\boldsymbol{x}^{(q)}\right)\boldsymbol{f}_{\mathrm{S}}^{(q)}\left(\boldsymbol{x}^{(q)}\right)^{\top}\right] = \boldsymbol{I},\ \mathbb{E}\left[\boldsymbol{f}_{\mathrm{S}}^{(q)}\left(\boldsymbol{x}^{(q)}\right)\right] = \boldsymbol{0},\ q=1,2, \tag{C.1c}$$

$$\boldsymbol{f}_{\mathrm{S}}^{(q)}\left(\boldsymbol{x}^{(q)}\right) \perp\!\!\!\perp \boldsymbol{f}_{\mathrm{P}}^{(q)}\left(\boldsymbol{x}^{(q)}\right),\ q=1,2, \tag{C.1d}$$

Again, under our generative model, any optimal solution $(\widehat{\boldsymbol{f}}^{(1)}, \widehat{\boldsymbol{f}}^{(2)})$ satisfies

$$\widehat{\boldsymbol{f}}_{\mathrm{S}}^{(1)}\left(\boldsymbol{x}^{(1)}\right) = \widehat{\boldsymbol{f}}_{\mathrm{S}}^{(2)}\left(\boldsymbol{x}^{(2)}\right).$$

We hope to further show that

$$\widehat{\boldsymbol{c}}^{(1)} = \widehat{\boldsymbol{f}}_{\mathrm{P}}\left(\boldsymbol{x}^{(1)}\right) = \boldsymbol{h}_{\mathrm{P}}^{(1)}\left(\begin{bmatrix}\boldsymbol{z}\\ \boldsymbol{c}^{(1)}\end{bmatrix}\right)$$

is an invertibe function-transformed version of $\boldsymbol{c}^{(1)}$.

Recall that we have the following Jacobian matrix for function $\boldsymbol{h}^{(1)}$

$$\boldsymbol{J}^{(1)} = \begin{bmatrix} \boldsymbol{J}_{11}^{(1)} & \boldsymbol{0} \\ \boldsymbol{J}_{21}^{(1)} & \boldsymbol{J}_{22}^{(1)} \end{bmatrix},$$

where the second row corresponding to function $\boldsymbol{h}_{\mathrm{P}}^{(1)}$.

Since we have shown that both $\left|\det \boldsymbol{J}_{11}^{(1)}\right| \neq 0$ and $\left|\det \boldsymbol{J}_{22}^{(1)}\right| \neq 0$ in Section B, we only need to show that $\boldsymbol{J}_{21}^{(1)}$ is an all-zero matrix. To show this, we will use the condition (C.1d). First, it is not hard to see that

$$\boldsymbol{J}_{21}^{(1)} = \begin{bmatrix} \frac{\partial\left[\boldsymbol{h}_{\mathrm{P}}^{(1)}\left(\boldsymbol{\omega}^{(1)}\right)\right]_1}{\partial \widehat{z}_1} & \cdots & \frac{\partial\left[\boldsymbol{h}_{\mathrm{P}}^{(1)}\left(\boldsymbol{\omega}^{(1)}\right)\right]_1}{\partial \widehat{z}_D} \\ \vdots & \ddots & \vdots \\ \frac{\partial\left[\boldsymbol{h}_{\mathrm{P}}^{(1)}\left(\boldsymbol{\omega}^{(1)}\right)\right]_{D_1}}{\partial \widehat{z}_1} & \cdots & \frac{\partial\left[\boldsymbol{h}_{\mathrm{P}}^{(1)}\left(\boldsymbol{\omega}^{(1)}\right)\right]_{D_1}}{\partial \widehat{z}_D} \end{bmatrix} \boldsymbol{J}_{11}^{(1)},$$

by chain rules where the first matrix on the right hand side is the Jacobian of $\widehat{\boldsymbol{c}}^{(1)}$ w.r.t. $\widehat{\boldsymbol{z}}$. By (C.1d), we have $\widehat{\boldsymbol{c}}^{(1)} \perp\!\!\!\perp \widehat{\boldsymbol{z}}$, which means that we can observe fixed $\tilde{\boldsymbol{c}}^{(1)} = (\widehat{c}_1^{(1)}, \cdots, \overline{c}_i, \cdots, \widehat{c}_{D_1}^{(1)})$ for any fixed $\overline{c}_i$ with any possible $\widehat{\boldsymbol{z}}$. Therefore, at any specific point of $\tilde{\boldsymbol{c}}^{(1)}$, the following always holds

$$\frac{\partial \left[\tilde{\boldsymbol{c}}^{(1)}\right]_i}{\partial \widehat{z}_j} = \frac{\partial \overline{c}_i}{\partial \widehat{z}_j} = 0,$$

since the numerator is a constant. Note that the above holds for any $\tilde{\boldsymbol{c}}^{(1)}$ with different $\overline{c}_i$ for $i \in [D_1]$, which further means that we actually have

$$\begin{bmatrix} \frac{\partial \left[\boldsymbol{h}_{\mathrm{P}}^{(1)}\left(\boldsymbol{\omega}^{(1)}\right)\right]_1}{\partial \widehat{z}_1} & \cdots & \frac{\partial \left[\boldsymbol{h}_{\mathrm{P}}^{(1)}\left(\boldsymbol{\omega}^{(1)}\right)\right]_1}{\partial \widehat{z}_D} \\ \vdots & \ddots & \vdots \\ \frac{\partial \left[\boldsymbol{h}_{\mathrm{P}}^{(1)}\left(\boldsymbol{\omega}^{(1)}\right)\right]_{D_1}}{\partial \widehat{z}_1} & \cdots & \frac{\partial \left[\boldsymbol{h}_{\mathrm{P}}^{(1)}\left(\boldsymbol{\omega}^{(1)}\right)\right]_{D_1}}{\partial \widehat{z}_D} \end{bmatrix} = \mathbf{0}$$

for all $\boldsymbol{h}_{\mathrm{P}}^{(1)}\left(\boldsymbol{\omega}^{(1)}\right)$ and $\widehat{\boldsymbol{z}}$.

Therefore, $\boldsymbol{J}_{21}^{(1)} = \mathbf{0}_{D_1 \times D} \boldsymbol{J}_{11}^{(1)} = \mathbf{0}_{D_1 \times D}$. Consequently, we have the following block diagonal form for $\boldsymbol{J}^{(1)}$ by combing with Theorem 1, i.e.,

$$\boldsymbol{J}^{(1)} = \begin{bmatrix} \boldsymbol{J}_{11}^{(1)} & \mathbf{0}_{D \times D_1} \\ \mathbf{0}_{D_1 \times D} & \boldsymbol{J}_{22}^{(1)} \end{bmatrix}.$$

By invertibility of $\widehat{\boldsymbol{f}}^{(q)}$ and $\boldsymbol{g}^{(q)}$, we have

$$\left|\det \boldsymbol{J}^{(1)}\right| = \left|\det \boldsymbol{J}_{11}^{(1)}\right| \left|\det \boldsymbol{J}_{22}^{(1)}\right| \neq 0,$$

which implies that $\widehat{\boldsymbol{z}} = \boldsymbol{\gamma}(\boldsymbol{z})$ and $\widehat{\boldsymbol{c}}^{(1)} = \boldsymbol{\delta}^{(1)}\left(\boldsymbol{c}^{(1)}\right)$ with invertible functions $\boldsymbol{\gamma}(\cdot)$ and $\boldsymbol{\delta}^{(1)}(\cdot)$, respectively. The similar proof technique applies to $\boldsymbol{\delta}^{(2)}(\cdot)$. □

D Proof of Theorem 3

Theorem 3. Under the generative model in (5) and Assumptions 1 and 2, assume that $(\boldsymbol{x}_\ell^{(1)}, \boldsymbol{x}_\ell^{(2)})$ for $\ell = 1, \ldots, N$ are i.i.d. samples of $(\boldsymbol{x}^{(1)}, \boldsymbol{x}^{(2)})$. Denote $\widehat{\boldsymbol{f}}^{(q)} \in \mathcal{F}$ as *any* solution of (6) with the invertibility constraint satisfied. Then, we have the following holds with probability of at least $1 - \delta$:

$$\mathbb{E}\left[\sum_{i=1}^{D}\sum_{j=1}^{D_q}\left(\partial\left[\widehat{\boldsymbol{f}}_{\mathrm{S}}\left(\boldsymbol{x}^{(q)}\right)\right]_i / \partial c_j^{(q)}\right)^2\right] = O\left(\left(D\mathfrak{R}_N + \sqrt{\log(1/\delta)/N} + \nu^2\right)^{2/3}\right) \tag{D.1}$$

for any $\boldsymbol{c}^{(q)} \in \mathcal{C}_q$ such that $-C_p + \kappa_j \leq c_j^{(q)} \leq C_p - \kappa_j$ for all $j \in [D_q]$ and all $i \in [D]$, where $\kappa_j = \Omega((3/C_d)^{1/3}(4C_f(2D\mathfrak{R}_N + C_f\sqrt{\log(1/\delta)/2N}) + 4\nu^2)^{1/6})$.

D.1 A Lemma on Rademacher complexity

To derive the Rademacher complexity of the loss function, we have the following lemma

Lemma 1 *Consider the following function class*

$$\mathcal{H} = \left\{ l\left(\boldsymbol{x}^{(1)}, \boldsymbol{x}^{(2)}\right) \middle| l\left(\boldsymbol{x}^{(1)}, \boldsymbol{x}^{(2)}\right) = \sum_{d=1}^{D}\left(\boldsymbol{f}_d^{(1)}\left(\boldsymbol{x}^{(1)}\right) - \boldsymbol{f}_d^{(2)}\left(\boldsymbol{x}^{(2)}\right)\right)^2 \right\}$$

where $\boldsymbol{f}_d^{(1)}, \boldsymbol{f}_d^{(2)} \in \mathcal{F}'$ are as defined in Assumption 2. Assume that $\left|\boldsymbol{f}_d^{(q)}\left(\boldsymbol{x}^{(q)}\right)\right| \leq C_f$ for all $\boldsymbol{f}_d^{(q)} \in \mathcal{F}'$, where $C_f > 0$. Then, the Rademacher complexity of class $\mathcal{H}$ is bounded by

$$\mathfrak{R}_N(\mathcal{H}) \leq 4DC_f\mathfrak{R}_N.$$

Proof: First, we have the function $\left|\boldsymbol{f}_d^{(1)}\left(\boldsymbol{x}^{(1)}\right)-\boldsymbol{f}_d^{(2)}\left(\boldsymbol{x}^{(2)}\right)\right|$ bounded within $[0, 2C_f]$. According to the Lipschitz composition property of Rademacher complexity (Bartlett & Mendelson, 2002), we have

$$\mathfrak{R}_N(\phi \circ \mathcal{F}) \leq L_\phi \mathfrak{R}_N(\mathcal{F})$$

where L_ϕ is the Lipschitz constant of ϕ. Here $\phi(x) = x^2$ and $L_\phi = 4C_f$.

Combining with the linearity property of the Rademacher complexity (Bartlett & Mendelson, 2002), we have

$$\mathfrak{R}_N(\mathcal{H}) \leq 4DC_f\mathfrak{R}_N \tag{D.2}$$

which completes the proof of the lemma. Note that (D.2) is derived by treating $\boldsymbol{f}_d^{(q)}$ for $d \in [D]$ as individual functions. However, $\boldsymbol{f}_d^{(q)}$ for $d \in [D]$ are the first D outputs of the same function $\boldsymbol{f}^{(q)}$—which means that many parameters of these D functions are constrained to be identical. Nonetheless, this fact does not affect the inequality in (D.2) since adding confining constraints to the function class $\mathcal{H}$ only reduces the Rademacher complexity (Bartlett & Mendelson, 2002). □

D.2 Proof of Theorem 3

First, we bound the true risk on the view matching loss. Consider the regression problem given $\left(\boldsymbol{x}_\ell^{(1)}, \boldsymbol{x}_\ell^{(2)}\right)$ as samples, we have

$$\underset{\boldsymbol{f}^{(1)},\boldsymbol{f}^{(2)}}{\text{minimize}} \ \frac{1}{N}\sum_{\ell=1}^{N}\left\|\boldsymbol{f}_{\mathrm{S}}^{(1)}\left(\boldsymbol{x}_\ell^{(1)}\right)-\boldsymbol{f}_{\mathrm{S}}^{(2)}\left(\boldsymbol{x}_\ell^{(2)}\right)\right\|_2^2.$$

By Lemma 1 and (Mohri et al., 2018, Theorem 3.3), we have the following hold with probability at least $1-\delta$

$$\begin{aligned}\mathbb{E}\left[\left\|\boldsymbol{f}_{\mathrm{S}}^{(1)}\left(\boldsymbol{x}_\ell^{(1)}\right)-\boldsymbol{f}_{\mathrm{S}}^{(2)}\left(\boldsymbol{x}_\ell^{(2)}\right)\right\|_2^2\right] &\leq \frac{1}{N}\sum_{\ell=1}^{N}\left\|\boldsymbol{f}_{\mathrm{S}}^{(1)}\left(\boldsymbol{x}_\ell^{(1)}\right)-\boldsymbol{f}_{\mathrm{S}}^{(2)}\left(\boldsymbol{x}_\ell^{(2)}\right)\right\|_2^2 \\ &\quad + 2\mathfrak{R}_N(\mathcal{H}) + 4C_f^2\sqrt{\frac{\log(1/\delta)}{2N}}.\end{aligned}$$

By Assumption 2(c), the first term on the right hand side can be bounded as

$$\begin{aligned}&\frac{1}{N}\sum_{\ell=1}^{N}\left\|\boldsymbol{f}_{\mathrm{S}}^{(1)}\left(\boldsymbol{x}_\ell^{(1)}\right)-\boldsymbol{f}_{\mathrm{S}}^{(2)}\left(\boldsymbol{x}_\ell^{(2)}\right)\right\|_2^2 \\ &= \frac{1}{N}\sum_{\ell=1}^{N}\left\|\boldsymbol{f}_{\mathrm{S}}^{(1)}\left(\boldsymbol{x}_\ell^{(1)}\right)-\boldsymbol{u}_{\mathrm{S}}^{(1)}\left(\boldsymbol{x}^{(1)}\right)+\boldsymbol{u}_{\mathrm{S}}^{(2)}\left(\boldsymbol{x}^{(2)}\right)-\boldsymbol{f}_{\mathrm{S}}^{(2)}\left(\boldsymbol{x}_\ell^{(2)}\right)\right\|_2^2 \\ &\leq \frac{1}{N}\sum_{\ell=1}^{N}(\nu+\nu)^2 = 4\nu^2.\end{aligned}$$

where the first equality is because there exist $\boldsymbol{u}^{(1)} \in \mathcal{G}^{-1}$ and $\boldsymbol{u}^{(2)} \in \mathcal{G}^{-1}$ such that $\boldsymbol{u}_{\mathrm{S}}^{(1)}\left(\boldsymbol{x}^{(1)}\right) = \boldsymbol{u}_{\mathrm{S}}^{(2)}\left(\boldsymbol{x}^{(2)}\right) = \boldsymbol{\gamma}(\boldsymbol{z})$ and the second inequality is by the triangle inequality.

Therefore, by plugging in $\mathfrak{R}_N(\mathcal{H})$ we have:

$$\mathbb{E}\left[\left\|\boldsymbol{f}_{\mathrm{S}}^{(1)}\left(\boldsymbol{x}_\ell^{(1)}\right)-\boldsymbol{f}_{\mathrm{S}}^{(2)}\left(\boldsymbol{x}_\ell^{(2)}\right)\right\|_2^2\right] \leq \epsilon$$

with the definition

$$\begin{aligned}\epsilon &:= 4\nu^2 + 8DC_f\mathfrak{R}_N + 4C_f^2\sqrt{\frac{\log(1/\delta)}{2N}} \\ &= 4C_f\left(2D\mathfrak{R}_N + C_f\sqrt{\frac{\log(1/\delta)}{2N}}\right) + 4\nu^2.\end{aligned}$$

Next, we use the bound of true risk to bound the energy of the entries of the Jacobian matrix on the left hand side of Eq. (D.1). Denote $\boldsymbol{h}_{\mathrm{S}}^{(q)} = \boldsymbol{f}_{\mathrm{S}}^{(q)} \circ \boldsymbol{g}^{(q)}$. We define the error for any individual sample pair $\left(\boldsymbol{x}_\ell^{(1)}, \boldsymbol{x}_\ell^{(2)}\right) \sim p\left(\boldsymbol{x}^{(1)}, \boldsymbol{x}^{(2)}\right)$ as

$$\left\|\boldsymbol{f}_{\mathrm{S}}^{(1)}(\boldsymbol{x}_\ell^{(1)}) - \boldsymbol{f}_{\mathrm{S}}^{(2)}(\boldsymbol{x}_\ell^{(2)})\right\|_2^2 = \varepsilon_\ell,$$

with $\mathbb{E}[\varepsilon_\ell] \leq \epsilon$.

Define another two pairs of samples, such that

$$\left\|\boldsymbol{h}_{\mathrm{S}}^{(1)}\left(\begin{bmatrix}\boldsymbol{z}_\ell \\ \boldsymbol{c}_\ell^{(1)} + \Delta \boldsymbol{e}_j\end{bmatrix}\right) - \boldsymbol{h}_{\mathrm{S}}^{(2)}\left(\begin{bmatrix}\boldsymbol{z}_\ell \\ \boldsymbol{c}_\ell^{(2)}\end{bmatrix}\right)\right\|_2^2 = \varepsilon_{\widehat{\ell}},$$
$$\left\|\boldsymbol{h}_{\mathrm{S}}^{(1)}\left(\begin{bmatrix}\boldsymbol{z}_\ell \\ \boldsymbol{c}_\ell^{(1)} - \Delta \boldsymbol{e}_j\end{bmatrix}\right) - \boldsymbol{h}_{\mathrm{S}}^{(2)}\left(\begin{bmatrix}\boldsymbol{z}_\ell \\ \boldsymbol{c}_\ell^{(2)}\end{bmatrix}\right)\right\|_2^2 = \varepsilon_{\tilde{\ell}},$$

where $\Delta > 0$ and $\boldsymbol{e}_j$ is the unit vector in the $c_j^{(1)}$ direction. Then by triangle inequality we have

$$\left\|\boldsymbol{h}_{\mathrm{S}}^{(1)}\left(\begin{bmatrix}\boldsymbol{z}_\ell \\ \boldsymbol{c}_\ell^{(1)} + \Delta \boldsymbol{e}_j\end{bmatrix}\right) - \boldsymbol{h}_{\mathrm{S}}^{(1)}\left(\begin{bmatrix}\boldsymbol{z}_\ell \\ \boldsymbol{c}_\ell^{(1)} - \Delta \boldsymbol{e}_j\end{bmatrix}\right)\right\|_2 \leq \sqrt{\varepsilon_{\widehat{\ell}}} + \sqrt{\varepsilon_{\tilde{\ell}}}.$$

Define

$$\psi_{ij}\left(c_j^{(1)}\right) := \left[\boldsymbol{h}_{\mathrm{S}}^{(1)}\left(\left[\bar{\boldsymbol{z}}^\top, \left(\bar{c}_1^{(1)}, \cdots, c_j^{(1)}, \cdots, \bar{c}_{D_1}^{(1)}\right)\right]^\top\right)\right]_i,$$

which is a scalar function of $c_j^{(1)}$ with fixed $\bar{\boldsymbol{z}}$ and $\bar{c}_k^{(1)}$ for $k \neq j$.

Then the element $\frac{\partial\left[\widehat{\boldsymbol{f}}_{\mathrm{S}}\left(\boldsymbol{x}^{(1)}\right)\right]_i}{\partial c_j^{(1)}}$ can be estimated using the central difference formula as

$$\begin{aligned}
\left|\frac{\partial\left[\widehat{\boldsymbol{f}}_{\mathrm{S}}\left(\boldsymbol{x}^{(1)}\right)\right]_i}{\partial c_j^{(1)}}\right| &= \left|\frac{\left[\boldsymbol{h}_{\mathrm{S}}^{(1)}\left(\begin{bmatrix}\boldsymbol{z}_\ell \\ \boldsymbol{c}_\ell^{(1)} + \Delta \boldsymbol{e}_j\end{bmatrix}\right) - \boldsymbol{h}_{\mathrm{S}}^{(1)}\left(\begin{bmatrix}\boldsymbol{z}_\ell \\ \boldsymbol{c}_\ell^{(1)} - \Delta \boldsymbol{e}_j\end{bmatrix}\right)\right]_i}{2\Delta} - \frac{\Delta^2}{12}\left(\psi_{ij}'''(\xi_1) + \psi_{ij}'''(\xi_2)\right)\right| \\
&\leq \frac{\left|\left[\boldsymbol{h}_{\mathrm{S}}^{(1)}\left(\begin{bmatrix}\boldsymbol{z}_\ell \\ \boldsymbol{c}_\ell^{(1)} + \Delta \boldsymbol{e}_j\end{bmatrix}\right) - \boldsymbol{h}_{\mathrm{S}}^{(1)}\left(\begin{bmatrix}\boldsymbol{z}_\ell \\ \boldsymbol{c}_\ell^{(1)} - \Delta \boldsymbol{e}_j\end{bmatrix}\right)\right]_i\right|}{2\Delta} + \left|\frac{\Delta^2}{6}\psi_{ij}'''(\xi')\right|,
\end{aligned}$$

where $\xi_1 \in \left(c_{\ell,j}^{(1)}, c_{\ell,j}^{(1)} + \Delta\right)$, $\xi_2 \in \left(c_{\ell,j}^{(1)} - \Delta, c_{\ell,j}^{(1)}\right)$ and by intermediate value theorem $\xi' \in \left(c_{\ell,j}^{(1)} - \Delta, c_{\ell,j}^{(1)} + \Delta\right)$.

Since $|x_i| \leq \|\boldsymbol{x}\|_\infty \leq \|\boldsymbol{x}\|_2$, we have

$$\left|\frac{\partial\left[\widehat{\boldsymbol{f}}_{\mathrm{S}}\left(\boldsymbol{x}^{(1)}\right)\right]_i}{\partial c_j^{(1)}}\right| \leq \frac{\sqrt{\varepsilon_{\widehat{\ell}}} + \sqrt{\varepsilon_{\tilde{\ell}}}}{2\Delta} + \left|\frac{\Delta^2}{6}\psi_{ij}'''(\xi')\right|.$$

By taking expectation, we have

$$\begin{aligned}
\mathbb{E}\left[\left|\frac{\partial\left[\widehat{\boldsymbol{f}}_{\mathrm{S}}\left(\boldsymbol{x}^{(1)}\right)\right]_i}{\partial c_j^{(1)}}\right|\right] &\leq \frac{\mathbb{E}[\sqrt{\varepsilon_{\widehat{\ell}}}] + \mathbb{E}[\sqrt{\varepsilon_{\tilde{\ell}}}]}{2\Delta} + \left|\frac{\Delta^2}{6}\psi_{ij}'''(\xi')\right| \\
&\leq \frac{\sqrt{\epsilon}}{\Delta} + \frac{\Delta^2}{6}|\psi_{ij}'''(\xi')|,
\end{aligned}$$

where the second inequality is by Jensen's inequality

$$\mathbb{E}[\sqrt{\varepsilon_\ell}] \leq \sqrt{\mathbb{E}[\varepsilon_\ell]} \leq \sqrt{\varepsilon},$$

due to the concavity of $\sqrt{x}$.

We aim to find the smallest upper bound, i.e.,

$$\inf_{0<\Delta<\min\left\{C_p+c_{\ell,j}^{(1)},C_p-c_{\ell,j}^{(1)}\right\}} \frac{\sqrt{\epsilon}}{\Delta}+\frac{\Delta^2}{6}|\psi_{ij}'''(\xi')|. \tag{D.3}$$

Note that the function in (D.3) is convex and smooth. We have the minimizer

$$\Delta^* \in \left\{\left(\frac{3\sqrt{\epsilon}}{|\psi_{ij}'''(\xi')|}\right)^{1/3}, \min\left\{C_p+c_{\ell,j}^{(1)}, C_p-c_{\ell,j}^{(1)}\right\}\right\},$$

which gives us the minimum

$$\inf_{\Delta} \frac{\sqrt{\epsilon}}{\Delta}+\frac{\Delta^2}{6}|\psi_{ij}'''(\xi')| \leq \min\left\{\frac{3}{2}\left(\frac{|\psi_{ij}'''(\xi')|}{3}\right)^{1/3}\epsilon^{1/3}, \frac{\sqrt{\epsilon}}{\kappa_j}+\frac{\kappa_j^2}{6}|\psi_{ij}'''(\xi')|\right\}.$$

where $\kappa_j = \min\left\{C_p+c_{\ell,j}^{(1)}, C_p-c_{\ell,j}^{(1)}\right\}$.

If $\kappa_j \geq \left(\frac{3\sqrt{\epsilon}}{|\psi_{ij}'''(\xi')|}\right)^{1/3}$, then we can bound

$$\mathbb{E}\left[\left|\frac{\partial\left[\widehat{\boldsymbol{f}}_{\mathrm{S}}\left(\boldsymbol{x}^{(1)}\right)\right]_i}{\partial c_j^{(1)}}\right|\right] \leq \frac{3}{2}\left(\frac{|\psi_{ij}'''(\xi')|}{3}\right)^{1/3}\epsilon^{1/3}.$$

With fixed N, one can choose $\epsilon = 4C_f\left(2D\mathfrak{R}_N + C_f\sqrt{\frac{\log(1/\delta)}{2N}}\right)+4\nu^2$, which gives the following bound

$$\mathbb{E}\left[\left|\frac{\partial\left[\widehat{\boldsymbol{f}}_{\mathrm{S}}\left(\boldsymbol{x}^{(1)}\right)\right]_i}{\partial c_j^{(1)}}\right|\right] \leq \frac{3}{2}\left(\frac{C_d}{3}\right)^{1/3}\left(4C_f\left(2D\mathfrak{R}_N + C_f\sqrt{\frac{\log(1/\delta)}{2N}}\right)+4\nu^2\right)^{1/3},$$

if $\kappa_j \geq \left(\frac{3}{C_d}\right)^{1/3}\left(4C_f\left(2D\mathfrak{R}_N + C_f\sqrt{\frac{\log(1/\delta)}{2N}}\right)+4\nu^2\right)^{1/6}$.

Considering all i, j pairs, we have

$$\mathbb{E}\left[\sum_{i=1}^{D}\sum_{j=1}^{D_1}\left|\frac{\partial\left[\widehat{\boldsymbol{f}}_{\mathrm{S}}\left(\boldsymbol{x}^{(1)}\right)\right]_i}{\partial c_j^{(1)}}\right|\right] \leq \frac{3}{2}DD_1\left(\frac{C_d}{3}\right)^{1/3}\left(4C_f\left(2D\mathfrak{R}_N + C_f\sqrt{\frac{\log(1/\delta)}{2N}}\right)+4\nu^2\right)^{1/3}.$$

Since $\|\cdot\|_2$ is upper bounded by $\|\cdot\|_1$, we have

$$\mathbb{E}\left[\sum_{i=1}^{D}\sum_{j=1}^{D_1}\left(\frac{\partial\left[\widehat{\boldsymbol{f}}_{\mathrm{S}}\left(\boldsymbol{x}^{(1)}\right)\right]_i}{\partial c_j^{(1)}}\right)^2\right] \leq \frac{9}{4}D^2D_1^2\left(\frac{C_d}{3}\right)^{2/3}\left(4C_f\left(2D\mathfrak{R}_N + C_f\sqrt{\frac{\log(1/\delta)}{2N}}\right)+4\nu^2\right)^{2/3},$$

which completes the proof. The same holds for $q = 2$ by role symmetry.

E Proof of Proposition 1

The claim can be proved by contradiction. Take $q = 1$ for example. Suppose that there exists two elements $\widehat{z}_i$ and $\widehat{c}_j^{(1)}$ that are dependent but (9) is 0. Let

$$\phi_1 = \boldsymbol{e}_i^\top, \quad \tau_1 = \boldsymbol{e}_j^\top,$$

which are valid choices. Then, we have

$$\mathbb{C}\mathrm{ov}[\phi_1(\widehat{\boldsymbol{z}})\tau_1(\widehat{\boldsymbol{c}}^{(1)})] = \mathbb{E}[\widehat{z}_i\widehat{c}_j^{(1)}] - \mathbb{E}[\widehat{z}_i]\mathbb{E}[\widehat{c}_j^{(1)}].$$

Note that by definition of independence, we have

$$\mathbb{E}[\widehat{z}_i\widehat{c}_j^{(1)}] = \mathbb{E}[\widehat{z}_i]\mathbb{E}[\widehat{c}_j^{(1)}] \Longleftrightarrow \widehat{z}_i \perp\!\!\!\perp \widehat{c}_j^{(1)}.$$

Hence, z_i and z_j being dependent means that

$$\mathbb{E}[\widehat{z}_i\widehat{c}_j^{(1)}] - \mathbb{E}[\widehat{z}_i]\mathbb{E}[\widehat{c}_j^{(1)}] \neq 0.$$

Consequently, one can see that

$$\sup_{\phi_1,\tau_1} \mathbb{C}\mathrm{ov}[\phi_1(\widehat{\boldsymbol{z}})\tau_1(\widehat{\boldsymbol{c}}^{(1)})] \geq \mathbb{C}\mathrm{ov}[\phi_1(\widehat{\boldsymbol{z}})\tau_1(\widehat{\boldsymbol{c}}^{(1)})]|_{\phi_1=\boldsymbol{e}_i^\top,\tau_1=\boldsymbol{e}_j^\top} = \mathbb{C}\mathrm{ov}[\widehat{z}_i\widehat{c}_j^{(1)}] \neq 0.$$

The above is a contradiction to our assumption that holds.

On the other hand, if $\widehat{z}_i$ and $\widehat{c}_j^{(1)}$ are independent for all $i \in [D]$ and $j \in [D_1]$, then we have

$$\mathbb{E}[\phi(\widehat{z}_i)\tau(\widehat{c}_j^{(1)})] - \mathbb{E}[\phi(\widehat{z}_i)]\mathbb{E}[\tau(\widehat{c}_j^{(1)})] = 0,$$

for all $i \in [D]$ and $j \in [D_1]$, for any $\phi : \mathbb{R} \to \mathbb{R}$ and $\tau : \mathbb{R} \to \mathbb{R}$.

F Detailed Algorithm Implementation

Recall that the proposed criterion is

$$\underset{\boldsymbol{f}^{(1)},\boldsymbol{f}^{(2)}}{\text{maximize}}\ \mathrm{Tr}\left(\frac{1}{N}\sum_{\ell=1}^{N}\boldsymbol{f}_{\mathrm{S}}^{(1)}\left(\boldsymbol{x}_\ell^{(1)}\right)\boldsymbol{f}_{\mathrm{S}}^{(2)}\left(\boldsymbol{x}_\ell^{(2)}\right)^\top\right) \tag{F.1a}$$

$$\text{subject to } \boldsymbol{f}^{(q)} \text{ for } q=1,2 \text{ are invertible,} \tag{F.1b}$$

$$\frac{1}{N}\sum_{\ell=1}^{N}\boldsymbol{f}_{\mathrm{S}}^{(q)}\left(\boldsymbol{x}_\ell^{(q)}\right)\boldsymbol{f}_{\mathrm{S}}^{(q)}\left(\boldsymbol{x}_\ell^{(q)}\right)^\top = \boldsymbol{I},\ \frac{1}{N}\sum_{\ell=1}^{N}\boldsymbol{f}_{\mathrm{S}}^{(q)}\left(\boldsymbol{x}_\ell^{(q)}\right) = \boldsymbol{0},\ q=1,2, \tag{F.1c}$$

$$\boldsymbol{f}_{\mathrm{S}}^{(q)}\left(\boldsymbol{x}_\ell^{(q)}\right) \perp\!\!\!\perp \boldsymbol{f}_{\mathrm{P}}^{(q)}\left(\boldsymbol{x}_\ell^{(q)}\right),\ q=1,2, \tag{F.1d}$$

We will use neural networks to parameterize the functions that we aim to learn. To move forward, first, as we have shown in the proof of Theorem 1, Eq. (F.1) is equivalent to the following:

$$\underset{\boldsymbol{f}^{(1)},\boldsymbol{f}^{(2)}}{\text{minimize}}\ \frac{1}{N}\sum_{\ell=1}^{N}\left\|\boldsymbol{f}_{\mathrm{S}}^{(1)}\left(\boldsymbol{x}_\ell^{(1)}\right)-\boldsymbol{f}_{\mathrm{S}}^{(2)}\left(\boldsymbol{x}_\ell^{(2)}\right)\right\|_2^2 \tag{F.2a}$$

$$\text{subject to } \frac{1}{N}\sum_{\ell=1}^{N}\boldsymbol{f}_{\mathrm{S}}^{(q)}\left(\boldsymbol{x}_\ell^{(q)}\right)\boldsymbol{f}_{\mathrm{S}}^{(q)}\left(\boldsymbol{x}_\ell^{(q)}\right)^\top = \boldsymbol{I},\ \frac{1}{N}\sum_{\ell=1}^{N}\boldsymbol{f}_{\mathrm{S}}^{(q)}\left(\boldsymbol{x}_\ell^{(q)}\right) = \boldsymbol{0},\ q=1,2 \tag{F.2b}$$

$$\boldsymbol{f}^{(q)} \text{ for } q=1,2 \text{ are invertible,} \tag{F.2c}$$

$$\boldsymbol{f}_{\mathrm{S}}^{(q)}\left(\boldsymbol{x}_\ell^{(q)}\right) \perp\!\!\!\perp \boldsymbol{f}_{\mathrm{P}}^{(q)}\left(\boldsymbol{x}_\ell^{(q)}\right),\ q=1,2, \tag{F.2d}$$

Note that we have manifold constraints on both neural networks $\boldsymbol{f}_{\mathrm{S}}^{(1)}$ and $\boldsymbol{f}_{\mathrm{S}}^{(2)}$. Directly optimizing over such manifold constraints may be costly and challenging. To reduce the difficulty of this constrained problem, we introduce a slack variable $\boldsymbol{u}_\ell$ and recast the formulation in (F.2) as follows:

$$\underset{\boldsymbol{f}^{(1)},\boldsymbol{f}^{(2)},\boldsymbol{u}_\ell}{\text{minimize}}\ \mathcal{L} = \frac{1}{N}\sum_{\ell=1}^{N}\mathcal{L}_\ell = \frac{1}{N}\sum_{\ell=1}^{N}\sum_{q=1}^{2}\left\|\boldsymbol{u}_\ell - \boldsymbol{f}_{\mathrm{S}}^{(q)}(\boldsymbol{x}_\ell^{(q)})\right\|_2^2 \tag{F.3a}$$

$$\text{subject to } \frac{1}{N}\sum_{\ell=1}^{N}\boldsymbol{u}_\ell\boldsymbol{u}_\ell^\top = \boldsymbol{I},\ \frac{1}{N}\sum_{\ell=1}^{N}\boldsymbol{u}_\ell = \boldsymbol{0}. \tag{F.3b}$$

$$\boldsymbol{f}^{(q)} \text{ for } q=1,2 \text{ are invertible,} \tag{F.3c}$$

$$\boldsymbol{f}_{\mathrm{S}}^{(q)}\left(\boldsymbol{x}_\ell^{(q)}\right) \perp\!\!\!\perp \boldsymbol{f}_{\mathrm{P}}^{(q)}\left(\boldsymbol{x}_\ell^{(q)}\right),\ q=1,2, \tag{F.3d}$$

Ideally, we hope that $\boldsymbol{u}_\ell = \boldsymbol{\gamma}(\boldsymbol{z}_\ell)$. Introducing $\boldsymbol{u}_\ell$ makes the $\boldsymbol{f}^{(1)}$ and $\boldsymbol{f}^{(2)}$ subproblems unconstrained. This is a commonly used reformulation in neural network based multiview matching (see (Benton et al., 2017; Lyu & Fu, 2020)), which is reminiscent of the MAX-VAR formulation of CCA (Kettenring, 1971; Carroll, 1968; Rastogi et al., 2015). Such reformulations oftentimes make algorithm design easier, since the constraints are simplified.

The inveritibility and independence constraints in (F.3c) and (F.3d) are also not straightforward to enforce. Instead of directly enforcing the invertibility constraint in (F.3c), we design a regularization term. Specifically, we use the idea of autoencoder that reconstructs the samples from their latent representations $\boldsymbol{f}^{(q)}(\boldsymbol{x}_\ell^{(q)})$. We define a regularizer

$$\mathcal{V} = \frac{1}{N}\sum_{\ell=1}^{N}\mathcal{V}_\ell = \frac{1}{N}\sum_{\ell=1}^{N}\sum_{q=1}^{2}\left\|\boldsymbol{x}_\ell^{(q)} - \boldsymbol{r}^{(q)}(\boldsymbol{f}^{(q)}(\boldsymbol{x}_\ell^{(q)}))\right\|_2^2, \tag{F.4}$$

as the reconstruction loss, where $\boldsymbol{r}^{(q)}$'s are the reconstruction neural networks. Note that the above term being zero does not necessarily indicate that the function $\boldsymbol{f}^{(q)}$ is invertible, since this term is only imposed on limited number of samples. But in practice, this idea is effective in learning invertible transformations—also see (Wang et al., 2015; Lyu & Fu, 2020).

To promote the statistical independence constraint in (F.3d), we use the designed independence regularizer, i.e.,

$$\sup_{\boldsymbol{\phi}^{(q)},\boldsymbol{\tau}^{(q)}} \mathcal{R}^{(q)} = \sup_{\boldsymbol{\phi}^{(q)},\boldsymbol{\tau}^{(q)}} \frac{\left|\mathbb{Cov}\left[\boldsymbol{\phi}^{(q)}(\widehat{\boldsymbol{z}})\boldsymbol{\tau}^{(q)}\left(\widehat{\boldsymbol{c}}^{(q)}\right)\right]\right|}{\left(\sqrt{\mathbb{V}[\boldsymbol{\phi}^{(q)}(\widehat{\boldsymbol{z}})]}\sqrt{\mathbb{V}\left[\boldsymbol{\tau}^{(q)}\left(\widehat{\boldsymbol{c}}^{(q)}\right)\right]}\right)}, \tag{F.5}$$

where $\boldsymbol{\phi}^{(q)}$ and $\boldsymbol{\tau}^{(q)}$ are again represented by neural networks.

Let $\boldsymbol{\theta}$ collect the parameters of $\boldsymbol{f}^{(q)}$ and $\boldsymbol{r}^{(q)}$, and $\boldsymbol{\eta}$ the parameters of $\boldsymbol{\phi}^{(q)}$ and $\boldsymbol{\tau}^{(q)}$. Putting all the terms together, our working cost function is summarized as follows:

$$\min_{\boldsymbol{U},\boldsymbol{\theta}} \max_{\boldsymbol{\eta}} \frac{1}{N}\sum_{\ell=1}^{N}\mathcal{L}_\ell(\boldsymbol{\theta},\boldsymbol{U}) + \beta\frac{1}{N}\sum_{\ell=1}^{N}\mathcal{V}_\ell(\boldsymbol{\theta}) + \lambda\mathcal{R}(\boldsymbol{\theta},\boldsymbol{\eta}), \tag{F.6a}$$

$$\text{subject to } \frac{1}{N}\sum_{\ell=1}^{N}\boldsymbol{U}\boldsymbol{U}^\top = \boldsymbol{I},\ \frac{1}{N}\boldsymbol{U}\boldsymbol{1} = \boldsymbol{0}, \tag{F.6b}$$

where $\boldsymbol{U} = [\boldsymbol{u}_1, \cdots, \boldsymbol{u}_N] \in \mathbb{R}^{D\times N}$, and β and λ are nonnegative and $\mathcal{R} = \sum_{q=1}^{2}\mathcal{R}^{(q)}$.

In terms of algorithm design, we propose to handle $\boldsymbol{U}$, $\boldsymbol{\theta}$ and $\boldsymbol{\eta}$ cyclically when the other two are fixed, i.e., alternating optimization (AO).

First, we use stochastic gradient descent and ascent for the unconstrained $\boldsymbol{\theta}$ and $\boldsymbol{\eta}$ subproblems. To proceed, we sample a batch of data indexed by $\mathcal{B} \subseteq [N]$. Then, $\boldsymbol{\theta}$ and $\boldsymbol{\eta}$ can be updated by any stochastic gradient based optimizers, e.g., the plain-vanilla stochastic gradient descent/ascent,

$$\boldsymbol{\theta} \leftarrow \boldsymbol{\theta} - \gamma\left(\frac{1}{|\mathcal{B}|}\sum_{\ell\in\mathcal{B}}(\nabla_{\boldsymbol{\theta}}\mathcal{L}_\ell(\boldsymbol{\theta},\boldsymbol{U}) + \beta\nabla_{\boldsymbol{\theta}}\mathcal{V}_\ell(\boldsymbol{\theta})) + \lambda\widehat{\nabla}_{\boldsymbol{\theta}}\mathcal{R}(\boldsymbol{\theta},\boldsymbol{\eta})\right),$$

$$\boldsymbol{\eta} \leftarrow \boldsymbol{\eta} + \delta\left(\lambda\widehat{\nabla}_{\boldsymbol{\eta}}\mathcal{R}(\boldsymbol{\theta},\boldsymbol{\eta})\right),$$

where γ and δ are the step sizes for the updates of $\boldsymbol{\theta}$ and $\boldsymbol{\eta}$, respectively. The stochastic gradients of $\mathcal{L}$, $\mathcal{V}$ are defined as follows:

$$\widehat{\nabla}_{\boldsymbol{\theta}}\mathcal{L} := \frac{1}{|\mathcal{B}|}\sum_{\ell\in\mathcal{B}}\nabla_{\boldsymbol{\theta}}\mathcal{L}_\ell(\boldsymbol{\theta},\boldsymbol{U}) \tag{F.7a}$$

$$\widehat{\nabla}_{\boldsymbol{\theta}}\mathcal{V} := \frac{1}{|\mathcal{B}|}\sum_{\ell\in\mathcal{B}}\nabla_{\boldsymbol{\theta}}\mathcal{V}_\ell(\boldsymbol{\theta}). \tag{F.7b}$$

In addition, the terms $\widehat{\nabla}_{\boldsymbol{\theta}}\mathcal{R}$ and $\widehat{\nabla}_{\boldsymbol{\eta}}\mathcal{R}$ are defined similarly. Taking the latter as an example. We have $\widehat{\nabla}_{\boldsymbol{\eta}}\mathcal{R} = \sum_{q=1}^{2}\widehat{\nabla}_{\boldsymbol{\eta}}\mathcal{R}^{(q)}$, and $\widehat{\nabla}_{\boldsymbol{\eta}}\mathcal{R}^{(q)}$ is estimated by taking gradient w.r.t. $\boldsymbol{\eta}$ of the following batch-estimated $\mathcal{R}^{(q)}$ (the same holds for $\widehat{\nabla}_{\boldsymbol{\theta}}\mathcal{R}$):

$$\mathcal{R}_{\mathcal{B}}^{(q)} := \frac{\left|\frac{1}{|\mathcal{B}|}\sum_{\ell\in\mathcal{B}}\left(\boldsymbol{\phi}^{(q)}(\widehat{\boldsymbol{z}}_\ell) - \frac{1}{|\mathcal{B}|}\sum_{\ell\in\mathcal{B}}\boldsymbol{\phi}^{(q)}(\widehat{\boldsymbol{z}}_\ell)\right)\left(\boldsymbol{\tau}^{(q)}\left(\widehat{\boldsymbol{c}}_\ell^{(q)}\right) - \frac{1}{|\mathcal{B}|}\sum_{\ell\in\mathcal{B}}\boldsymbol{\tau}^{(q)}\left(\widehat{\boldsymbol{c}}_\ell^{(q)}\right)\right)\right|}{\sqrt{\frac{1}{|\mathcal{B}|}\sum_{\ell\in\mathcal{B}}\left(\boldsymbol{\phi}^{(q)}(\widehat{\boldsymbol{z}}_\ell) - \frac{1}{|\mathcal{B}|}\sum_{\ell\in\mathcal{B}}\boldsymbol{\phi}^{(q)}(\widehat{\boldsymbol{z}}_\ell)\right)^2}\sqrt{\frac{1}{|\mathcal{B}|}\sum_{\ell\in\mathcal{B}}\left(\boldsymbol{\tau}^{(q)}\left(\widehat{\boldsymbol{c}}_\ell^{(q)}\right) - \frac{1}{|\mathcal{B}|}\sum_{\ell\in\mathcal{B}}\boldsymbol{\tau}^{(q)}\left(\widehat{\boldsymbol{c}}_\ell^{(q)}\right)\right)^2}} \tag{F.8a}$$

$$\widehat{\nabla}_{\boldsymbol{\eta}}\mathcal{R}^{(q)} := \nabla_{\boldsymbol{\eta}}\mathcal{R}_{\mathcal{B}}^{(q)} \tag{F.8b}$$

$$\widehat{\nabla}_{\boldsymbol{\theta}}\mathcal{R}^{(q)} := \nabla_{\boldsymbol{\theta}}\mathcal{R}_{\mathcal{B}}^{(q)}. \tag{F.8c}$$

It was shown in (Fisher, 1915) that the correlation coefficient is computed using random samples of Gaussian variables, the estimator in (F.8a) for $\mathcal{R}^{(q)}$ is asymptotically unbiased. For other distributions, the estimation also works well in practice; see, e.g., DCCA based works in (Wang et al., 2015).

Consider more general stochastic optimizers, e.g., Adam (Kingma & Ba, 2014) and Adagrad (Duchi et al., 2011). Then, the updates can be summarized as follows:

$$\boldsymbol{\theta} \leftarrow \texttt{SGD_optimizer}\left(\boldsymbol{\theta}, \widehat{\nabla}_{\boldsymbol{\theta}}\mathcal{L} + \beta\widehat{\nabla}_{\boldsymbol{\theta}}\mathcal{V} + \lambda\widehat{\nabla}_{\boldsymbol{\theta}}\mathcal{R}\right) \tag{F.9}$$

$$\boldsymbol{\eta} \leftarrow \texttt{SGD_optimizer}\left(\boldsymbol{\eta}, -\widehat{\nabla}_{\boldsymbol{\eta}}\mathcal{R}\right). \tag{F.10}$$

where (F.10) uses the negative stochastic gradient since it is an ascending step, while stochastic optimizers are by default descending the objective function.

The $\boldsymbol{U}$ subproblem consists of (F.3a) and (F.3b). It can be re-expressed as follows by expanding (F.3a):

$$\begin{aligned}&\frac{1}{N}\sum_{\ell=1}^{N}\sum_{q=1}^{2}\left\|\boldsymbol{u}_\ell - \boldsymbol{f}_{\mathrm{S}}^{(q)}(\boldsymbol{x}_\ell^{(q)})\right\|_2^2\\ =&\frac{1}{N}\sum_{\ell=1}^{N}\mathrm{Tr}\left(2\boldsymbol{u}_\ell\boldsymbol{u}_\ell^\top - 2\boldsymbol{u}_\ell\left(\boldsymbol{f}_{\mathrm{S}}^{(1)}\left(\boldsymbol{x}_\ell^{(1)}\right) + \boldsymbol{f}_{\mathrm{S}}^{(2)}\left(\boldsymbol{x}_\ell^{(2)}\right)\right)^\top + \sum_{q=1}^{2}\boldsymbol{f}_{\mathrm{S}}^{(q)}\left(\boldsymbol{x}_\ell^{(q)}\right)\boldsymbol{f}_{\mathrm{S}}^{(q)}\left(\boldsymbol{x}_\ell^{(q)}\right)^\top\right).\end{aligned}$$

Note that the first term is a constant by (F.3b) and the last term does not involve $\boldsymbol{u}_\ell$. Then, we rewrite the $\boldsymbol{u}_\ell$ subproblem as

$$\begin{aligned}\underset{\boldsymbol{U}}{\text{maximize}}\ &\mathrm{Tr}\left(\boldsymbol{U}\left(\boldsymbol{F}^{(1)} + \boldsymbol{F}^{(2)}\right)\right),\\ \text{subject to}\ &\frac{1}{N}\boldsymbol{U}\boldsymbol{U}^\top = \boldsymbol{I},\ \frac{1}{N}\boldsymbol{U}\boldsymbol{1} = \boldsymbol{0},\end{aligned} \tag{F.11}$$

where $\boldsymbol{F}^{(q)} = \left[\boldsymbol{f}_{\mathrm{S}}^{(q)}(\boldsymbol{x}_1^{(q)}), \cdots, \boldsymbol{f}_{\mathrm{S}}^{(q)}(\boldsymbol{x}_N^{(q)})\right]$. This is an orthogonal projection onto the set of row zero-mean and orthogonal matrices. It is shown in (Lyu & Fu, 2020, Lemma 1) that such a projection problem, although nonconvex, can be solved to optimality via a mean-removed singular value decomposition (SVD) procedure, i.e.,

$$\boldsymbol{U} \leftarrow \sqrt{N}\boldsymbol{S}\boldsymbol{T}^\top,\ \text{with}\ \boldsymbol{S}\boldsymbol{D}\boldsymbol{T}^\top = \mathrm{SVD}\left(\left(\boldsymbol{F}^{(1)} + \boldsymbol{F}^{(2)}\right)\boldsymbol{W}\right), \tag{F.12}$$

where $\boldsymbol{W} = \boldsymbol{I}_N - \frac{1}{N}\boldsymbol{1}\boldsymbol{1}^\top$ removes the mean of $\boldsymbol{F}^{(1)} + \boldsymbol{F}^{(2)}$, $\boldsymbol{D} \in \mathbb{R}^{D\times D}$ holds the singular values, $\boldsymbol{S} \in \mathbb{R}^{D\times D}$ and $\boldsymbol{T} \in \mathbb{R}^{N\times D}$ are the left and right orthogonal matrices in the SVD, respectively.

To summarize, an alternating optimization algorithm is summarized in Algorithm 1. Notice that we use two different batch sizes (denoted as $\mathcal{B}_1$ and $\mathcal{B}_2$ in line 4 of Algorithm 1) to construct the gradient estimations for $\widehat{\nabla}_{\boldsymbol{\theta}}\mathcal{L}$, $\widehat{\nabla}_{\boldsymbol{\theta}}\mathcal{V}$ and $\widehat{\nabla}_{\boldsymbol{\theta}}\mathcal{R}$, $\widehat{\nabla}_{\boldsymbol{\eta}}\mathcal{R}$, respectively. The reason is that accurately estimating of $\mathcal{R}$ using (F.8a) often requires a relatively large batch size, while small batches may suffice for the gradient estimations of $\mathcal{L}$ and $\mathcal{V}$, according to our extensive simulations.

Algorithm 1: Proposed Algorithm.

Data: $\boldsymbol{x}_\ell^{(q)}$ for $\ell = 1, \cdots, N$ and $q = 1, 2$
Result: $\boldsymbol{f}^{(q)}$, $\boldsymbol{r}^{(q)}$

while *stopping criterion is not reached* **do**
  $\boldsymbol{U} \leftarrow \sqrt{N}\boldsymbol{S}\boldsymbol{T}^\top$ with $\boldsymbol{S}\boldsymbol{D}\boldsymbol{T}^\top = \text{SVD}\left(\left(\boldsymbol{F}^{(1)} + \boldsymbol{F}^{(2)}\right)\boldsymbol{W}\right)$;
  while *stopping criterion is not reached* **do**
    draw a random batch $\mathcal{B}_1$ and $\mathcal{B}_2$; `// use` $|\mathcal{B}_2| > |\mathcal{B}_1|$
    $\widehat{\nabla}_{\boldsymbol{\theta}}\mathcal{L} \leftarrow \frac{1}{|\mathcal{B}_1|}\sum_{\ell\in\mathcal{B}_1}\nabla_{\boldsymbol{\theta}}\mathcal{L}_\ell$;
    $\widehat{\nabla}_{\boldsymbol{\theta}}\mathcal{V} \leftarrow \frac{1}{|\mathcal{B}_1|}\sum_{\ell\in\mathcal{B}_1}\nabla_{\boldsymbol{\theta}}\mathcal{V}_\ell$;
    $\widehat{\nabla}_{\boldsymbol{\eta}}\mathcal{R} \leftarrow \sum_{q=1}^{2}\nabla_{\boldsymbol{\eta}}\mathcal{R}_{\mathcal{B}_2}^{(q)}$; `// using` $\mathcal{B}_2$ `and` (F.8a), (F.8b)
    $\widehat{\nabla}_{\boldsymbol{\theta}}\mathcal{R} \leftarrow \sum_{q=1}^{2}\nabla_{\boldsymbol{\theta}}\mathcal{R}_{\mathcal{B}_2}^{(q)}$; `// using` $\mathcal{B}_2$ `and` (F.8a), (F.8c)
    $\boldsymbol{\theta} \leftarrow$ `SGD_optimizer` $\left(\boldsymbol{\theta}, \widehat{\nabla}_{\boldsymbol{\theta}}\mathcal{L} + \beta\widehat{\nabla}_{\boldsymbol{\theta}}\mathcal{V} + \lambda\widehat{\nabla}_{\boldsymbol{\theta}}\mathcal{R}\right)$; `// descent`
    $\boldsymbol{\eta} \leftarrow$ `SGD_optimizer` $\left(\boldsymbol{\eta}, -\lambda\widehat{\nabla}_{\boldsymbol{\eta}}\mathcal{R}\right)$; `// ascent`
  end
end

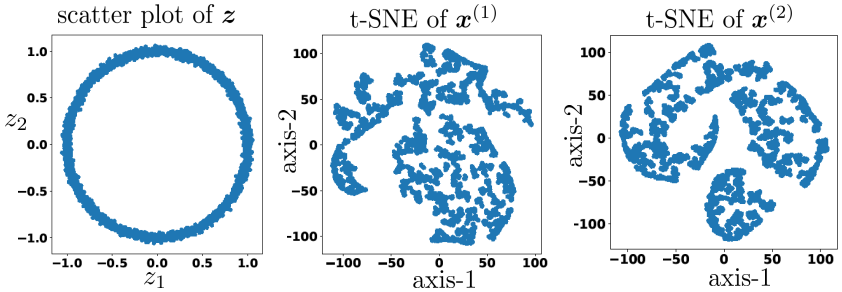

Figure G.1: Left: $\boldsymbol{z}$; middle: t-SNE of $\boldsymbol{x}^{(1)}$; right: t-SNE of $\boldsymbol{x}^{(2)}$.

G Experiments: More Details and Additional Validations

In this section, we show all the experiment results with greater details, e.g., results under more metrics, more setting details, and more demonstrations. We also include more real data experiments using the CIFAR10 (Krizhevsky et al., 2009) and dSprites data (Higgins et al., 2017).

G.1 Synthetic Data - Validating Main Theorems

In this subsection, we describe the synthetic data experiments. For synthetic data, we generate the shared $\boldsymbol{z} \in \mathbb{R}^2$ that is uniformly drawn from the unit circle, with noise $\mathcal{N}(0, 0.02^2)$ added to each dimension. The private components are scalars $c^{(1)} \sim \mathcal{N}(0, 2.0)$ and $c^{(2)} \sim \text{Laplace}(0, 4.0)$. The shared-to-private energy ratios for the two views are approximately -6 dB and -18 dB. The sample size is $N = 5,000$. And we use two different one-hidden-layer neural networks with 3 neurons and softplus activation to represent the invertible $\boldsymbol{g}^{(q)}$'s. The network parameters are drawn from standard normal distribution.

The shared component $\boldsymbol{z}$ and the t-SNE of $\boldsymbol{x}^{(1)}$ and $\boldsymbol{x}^{(2)}$ are shown in Fig. G.1. One can see that by incorporating strong noise and nonlinear transformations, the shape of circle is hardly to be identified in both views.

In our simulations, $\boldsymbol{f}^{(q)}$ is represented by a three-hidden-layer multi-layer perceptrons (MLPs) with 256 neurons in each layer with ReLU activations. In addition, $\boldsymbol{\phi}^{(q)}$ and $\boldsymbol{\tau}^{(q)}$ are represented by two-hidden-layer MLPs with 128 neurons in each layer. We set batch size to be 1000, $\beta = 1.0$, $\lambda = 0.1$. We use the Adam optimizer (Kingma & Ba, 2014) with initial learning rate 0.001 for all the parameters. Besides, we also regularize the network parameters using $\|\boldsymbol{\eta}\|_2^2$ with a regularization parameter

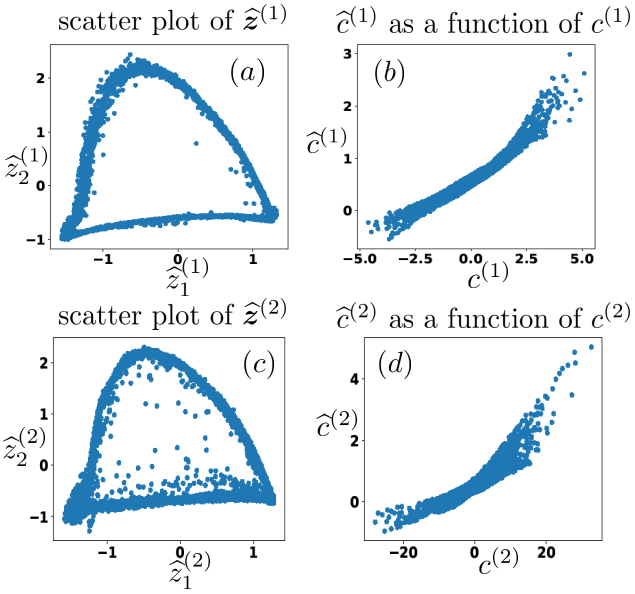

Figure G.2: (a) Scatter plot of $\widehat{\boldsymbol{z}}^{(1)}$; (b) $\widehat{c}^{(1)}$ as a function of $c^{(1)}$; (c) Scatter plot of $\widehat{\boldsymbol{z}}^{(2)}$; (d) $\widehat{c}^{(2)}$ as a function of $c^{(2)}$.

0.1. This often helps improve numerical stability when optimizing cost functions involving neural networks. We run lines 4-10 of Algorithm 1 for 10 epochs to update $\boldsymbol{\theta}$ and $\boldsymbol{\eta}$.

For ablation study, we test the methods with different combinations of $\mathcal{L}$, $\mathcal{R}$ and $\mathcal{V}$, i.e.,

(i) the proposed method ($\mathcal{L} + \mathcal{V} + \mathcal{R}$);

(ii) the proposed without independence regularization ($\mathcal{L} + \mathcal{V}$);

(iii) the proposed without reconstruction ($\mathcal{L} + \mathcal{R}$);

(iv) the proposed with only latent correlation maximization ($\mathcal{L}$);

(v) we also test the performance with HSIC (Lopez et al., 2018) as the independence regularizer ($\mathcal{L} + \mathcal{V} + \texttt{HISC}$);

All methods stop when the average matching loss $\mathcal{L}$ reaches 0.01. The learned components by the proposed method are shown in Fig. G.2. One can see that the estimated shared components are matched, while the second view exhibits relatively large noise level as expected. For the estimated private components, one can see that both $\delta^{(1)}(\cdot)$ and $\delta^{(2)}(\cdot)$ are approximately invertible functions.

To evaluate the performance of the synthetic experiment, we compute mutual information (MI) between groups of random variables of interest (measured by the mutual information neural estimation (MINE) (Belghazi et al., 2018) and Gaussian kernel density estimation (KDE) (Davis et al., 2011)). The results are averaged from 10 random trials.

One can see that all methods successfully extract the information about $\boldsymbol{z}$ in the sense that both $\widehat{\boldsymbol{z}}^{(q)} = \widehat{\boldsymbol{f}}_{\mathrm{S}}^{(q)}(\boldsymbol{x}^{(q)})$ for $q = 1, 2$ have similarly high MIs with $\boldsymbol{z}$. Besides, all methods output $\widehat{\boldsymbol{z}}^{(q)}$ and $\widehat{c}^{(q)}$ ($c^{(q)}$) that have small MIs—meaning that they are not dependent.

Although most loss functions using latent correlation maximization extract the shared $\boldsymbol{z}$'s information well, the difference is articulated in extracting the private information. The proposed $\mathcal{L}+\mathcal{V}+\mathcal{R}$ objective has the best performance on that regard. The method $\mathcal{L}+\mathcal{V}+\texttt{HSIC}$ also works reasonably well since $\texttt{HSIC}$ serves the same purpose as $\mathcal{R}$ does—but with a kernel-based implementation.

Moreover, by looking at the last two columns, one can see that the methods with $\mathcal{R}$ and $\mathcal{V}$ perform the best in removing the information of $\boldsymbol{z}$ from $c^{(q)}$. This corroborates our analysis that both (6b)

Table G.1: Mutual information (MI) between groups of variables. "↑": high score preferred; "↓": low score preferred; "n/a": not applicable; $\widehat{\boldsymbol{z}}^{(q)} = \widehat{\boldsymbol{f}}_{\mathrm{S}}^{(q)}$ for $q = 1, 2$.

	$\widehat{\boldsymbol{z}}^{(1)}$,$\boldsymbol{z}$ (↑)	$\widehat{\boldsymbol{z}}^{(2)}$,$\boldsymbol{z}$ (↑)	$\widehat{\boldsymbol{z}}^{(1)}$,$c^{(1)}$ (↓)	$\widehat{\boldsymbol{z}}^{(2)}$,$c^{(2)}$ (↓)	$\widehat{c}^{(1)}$,$c^{(1)}$ (↑)	$\widehat{c}^{(2)}$,$c^{(2)}$ (↑)	$\widehat{c}^{(1)}$,$\boldsymbol{z}$ (↓)	$\widehat{c}^{(2)}$,$\boldsymbol{z}$ (↓)
Metric	MINE-based MI Estimation (Belghazi et al., 2018)							
$\mathcal{L}$	2.32±0.06	2.36±0.10	0.01±0.00	0.00±0.00	0.45±0.13	0.33±0.07	0.39±0.14	0.43±0.04
$\mathcal{L}+\mathcal{V}$	2.37±0.05	2.38±0.08	0.01±0.00	0.01±0.00	0.55±0.09	0.33±0.08	0.31±0.06	0.43±0.05
$\mathcal{L}+\mathcal{R}$	2.32±0.05	2.33±0.07	0.02±0.01	0.00±0.00	0.90±0.42	0.22±0.12	0.09±0.06	0.22±0.12
$\mathcal{L}+\mathcal{V}+\mathcal{R}$	2.43±0.04	2.39±0.09	0.01±0.01	0.01±0.00	1.22± 0.33	0.85±0.23	0.04±0.02	0.11±0.03
$\mathcal{L}+\mathcal{V}$+HSIC	2.48±0.09	2.43±0.08	0.01±0.00	0.01±0.01	0.68±0.25	0.52±0.14	0.04±0.01	0.07±0.02
Metric	Gaussian kernel density estimate (KDE)-based MI Estimation							
$\mathcal{L}$	2.73±0.22	2.88±0.22	0.00±0.00	0.00	0.33±0.13	0.01±0.02	0.34±0.13	0.37±0.06
$\mathcal{L}+\mathcal{V}$	2.95±0.21	2.91±0.26	0.00±0.01	0.00	0.38±0.11	0.01±0.02	0.24±0.04	0.39±0.07
$\mathcal{L}+\mathcal{R}$	2.83±0.18	2.86±0.15	0.00	0.00	0.72±0.40	0.10±0.10	0.08±0.07	0.28±0.16
$\mathcal{L}+\mathcal{V}+\mathcal{R}$	3.27±0.07	2.88±0.25	0.00±0.01	0.00	0.99±0.30	0.35±0.11	0.03±0.04	0.08±0.03
$\mathcal{L}+\mathcal{V}$+HSIC	3.35±0.16	2.95±0.33	0.00	0.00	0.78±0.22	0.06±0.06	0.05±0.02	0.02±0.01

Table G.2: Mutual information (MI) between groups of variables under different SPR. "↑": high score preferred; "↓": low score preferred; $\widehat{\boldsymbol{z}}^{(q)} = \widehat{\boldsymbol{f}}_{\mathrm{S}}^{(q)}$ for $q = 1, 2$.

	$\widehat{\boldsymbol{z}}^{(1)}$,$\boldsymbol{z}$ (↑)	$\widehat{\boldsymbol{z}}^{(2)}$,$\boldsymbol{z}$ (↑)	$\widehat{\boldsymbol{z}}^{(1)}$,$c^{(1)}$ (↓)	$\widehat{\boldsymbol{z}}^{(2)}$,$c^{(2)}$ (↓)	$\widehat{c}^{(1)}$,$c^{(1)}$ (↑)	$\widehat{c}^{(2)}$,$c^{(2)}$ (↑)	$\widehat{c}^{(1)}$,$\boldsymbol{z}$ (↓)	$\widehat{c}^{(2)}$,$\boldsymbol{z}$ (↓)
SPR	MINE-based MI Estimation (Belghazi et al., 2018)							
-10 dB	2.41±0.07	2.43±0.05	0.01±0.01	0.01±0.01	1.72±0.41	0.52±0.10	0.02±0.01	0.19±0.03
-20 dB	1.81±0.10	2.15±0.09	0.10±0.06	0.01±0.01	1.41±0.15	1.15±0.07	0.08±0.04	0.06±0.02
-30 dB	1.16±0.07	1.55±0.10	0.11±0.09	0.07±0.04	1.77±0.42	0.73±0.14	0.03±0.02	0.14±0.11

(invertibility) and (6d) (independence) are vital to achieve private-shared information disentanglement.

Tab. G.1 shows the results, with all the entries averaged over 10 random trials. One can see that the results via the Gaussian KDE are consistent with those under MINE. That is, the proposed $\mathcal{L}+\mathcal{V}+\mathcal{R}$ exhibits the best performance in terms of extracting and disentangling the shared and private information.

G.2 Synthetic Data - Robustness to Strong Private Inteference

In this subsection, we demonstrate the performance of the proposed method under different levels of private component energy (which are often considered interference) (Ibrahim & Sidiropoulos, 2020; Bach & Jordan, 2005; Lyu & Fu, 2020). First, we define the *shared-to-private ratio* (SPR) for the q-th view as

$$\mathrm{SPR} = 10\log_{10}\left(\frac{\frac{1}{DN}\sum_{\ell=1}^{N}\|\boldsymbol{z}_\ell\|_2^2}{\frac{1}{D_qN}\sum_{\ell=1}^{N}\|\boldsymbol{c}_\ell^{(q)}\|_2^2}\right)\ \mathrm{dB}.$$

For the experiment, we make both views have identical SPRs. We test the performance under SPR=-10 dB, -20 dB and -30 dB, respectively.

Tab. G.2 shows the evaluation results averaged from 10 trials. One can see that as SPR decreases, the MI between the extracted $\widehat{\boldsymbol{z}}$ and $\boldsymbol{z}$ decreases—but only gracefully. The slight decline of performance is because the matching of two views becomes harder when the private components get stronger. However, even if SPR=-30 dB, the extraction and disentanglement of private and shared information are still clearly achieved. Such robustness to strong private interference is considered a key feature of linear CCA (Ibrahim & Sidiropoulos, 2020) and post-nonlinear CCA (Lyu & Fu, 2020). Our analysis and evaluation in this work show that such resilience is also inherited by the proposed approach.

G.3 Real Data - More on Validating Theorem 1

Multiview MNIST Data. In this subsection, we provide more details and evaluation results on the MNIST experiment. The way of generating such two views (as shown in Fig. 1 of the main text) of

Table G.3: Network structures for the MNIST experiment.

Encoders	Decoders
input: $\boldsymbol{x}_\ell^{(q)} \in \mathbb{R}^{28\times 28\times 1}$	input: $\boldsymbol{f}^{(q)}(\boldsymbol{x}_\ell^{(q)}) \in \mathbb{R}^{D+D_q}$
4×4 Conv, 64 ReLU, stride 2	FC 256, ReLU
4×4 Conv, 32 ReLU, stride 2	FC $7\times 7\times 32$, ReLU
FC 256, ReLU	4×4 Conv_Trans, 64 ReLU, stride 2
FC $D+D_q$	4×4 Conv_Trans, 1, stride 2

Table G.4: The classification error (first row) and clustering results (rows 2 to 4) of the two-view MNIST dataset. "↑": high score preferred; "↓": low score preferred.

	Baseline	$\mathcal{L}+\mathcal{V}+\mathcal{R}$	$\mathcal{L}+\mathcal{V}$	DCCA	DCCAE	`Barlow Twins`	`BYOL`
ERR (↓)	13.40%	2.81%±0.21%	2.95%±0.23%	2.87%±0.16%	2.85%±0.05%	2.05%±0.07%	2.67%±0.22%
ACC (↑)	37.35%	97.03%±0.13%	96.80%±0.40%	97.02%%±0.12%	96.95%±0.12%	98.06%±0.06%	95.56%±0.41%
NMI (↑)	0.337	0.922±0.003	0.923±0.007	0.922±0.003	0.920±0.003	0.947±0.002	0.895±0.023
ARI (↑)	0.216	0.936±0.003	0.931±0.009	0.935±0.003	0.934±0.002	0.958±0.001	0.904±0.047

MNIST data is similar to the data augmentation ideas used in AM-SSL, e.g., rotation, adding noise, cropping, flipping (Chen et al., 2020; Grill et al., 2020). We aim to match the two views and try to learn the shared representations, which should encode the class label information. The dataset has 70,000 samples that are 28×28 images of handwritten digits. For the latent dimension, we set $D = 10$, $D_1 = 20$ and $D_2 = 50$. In particular, since the second view consists of large random noise that are not of interest, we only add the independence regularizer $\mathcal{R}^{(1)}$ on the first view (i.e., the rotated digits) to learn the private component of $\boldsymbol{x}_\ell^{(1)}$. The learned $\widehat{\boldsymbol{c}}_\ell^{(1)}$ was used to generate new samples; see the illustration in our main text.

The network structure used for all methods is shown in Tab. G.3. The network structure for $\boldsymbol{\phi}^{(q)}$ and $\boldsymbol{\tau}^{(q)}$ are MLPs with three hidden layers of 64 neurons. For hyperparameters, we set batch size to be $|\mathcal{B}_1| = 100$ and $|\mathcal{B}_2| = 1000$, $\beta = 1.0$, $\lambda = 100.0$. For optimizer, we also use Adam (Kingma & Ba, 2014) with initial learning rate 0.001 for $\boldsymbol{\theta}$ and 1.0 for $\boldsymbol{\eta}$. And we add squared ℓ_2 regularization for both $\boldsymbol{\theta}$ and $\boldsymbol{\eta}$, with different regularization parameters that are 0.0001 and 0.1, respectively. We also run the SGD optimizer for 10 epochs to update $\boldsymbol{\theta}$ and $\boldsymbol{\eta}$.

In Tab. G.4, we show more evaluation results on the learned shared information across views. To be specific, we feed the learned $\widehat{\boldsymbol{z}}_\ell^{(1)}$'s to a classifier and the k-means algorithm, to observe if the learned representations improve the performance of supervised and unsupervised learning tasks. For the classification task, we split the data as 50,000/10,000/10,000 for training/validation/test sets. We train a linear support vector machine (SVM) using the training data. The performance is measured by classification error (ERR). For the clustering task, we use the standard k-means to cluster on all the data samples. After clustering, we report the performance on the test set. We use a number of metrics to measure performance, namely, clustering accuracy (ACC), normalized mutual information (NMI), and adjusted Rand index (ARI) (Yeung & Ruzzo, 2001). Among these metrics, ARI ranges from -1 to $+1$, with 1 being the best and -1 the worst and NMI range from 0 to 1 with 1 being the best.

The "Baseline" denotes the results of simply applying SVM and k-means onto the raw data of the first view, i.e., $\boldsymbol{x}_\ell^{(1)}$ for $\ell = 1, \ldots, N$. All the results of algorithms that involve stochastic methods are averaged over 5 random initializations. One can see that all methods have comparably good results in terms of learning informative representations across views. The results empirically validate our Theorem 1 that latent correlation maximization is a useful criterion to extract the shared information with guarantees. In particular, `Barlow Twins` performs slightly better in terms of benefiting downstream classification and clustering tasks. Nonetheless, the proposed method can also guarantee extracting private information and facilitate cross-view image generation (see the experiments in the main text), which is out the reach of `Barlow Twins` and `BYOL`.

Augmented CIFAR10 Data for SSL. We also use the CIFAR10 dataset (Krizhevsky et al., 2009) to validate Theorem 1. The CIFAR10 dataset contains 50,000 and 10,000 images of size 32×32 for training and testing, respectively. There are 10 different classes. We use ResNet18 as the backbone network for learning the representation. Since CIFAR10 images are small, we replace the first 7x7 Conv layer of stride 2 with 3x3 Conv layer of stride 1. We also remove the max pooling layer. We

Table G.5: Augmentation Used for CIFAR10 to Generate Multiple Views.

Transformation	Value	Probability
ColorJitter	brightness=0.8, contrast=0.8, saturation=0.8, hue=0.2	0.8
GrayScale	-	0.2
RandomResizedCrop	scale=(0.2, 1.0), ratio=(0.75, 4/3)	-
HorizontalFlip	-	0.5
GaussianBlur	$\sigma \sim U[0.1, 2]$	0.5
Solarization	-	0.4
Normalization	-	-

Table G.6: Evaluation using CIFAR10.

	BYOL	Barlow Twins	Proposed
Classification Acc. (%)	84.2	82.8	84.2
KNN ($k = 5$) Acc. (%)	80.5	78.7	81.0

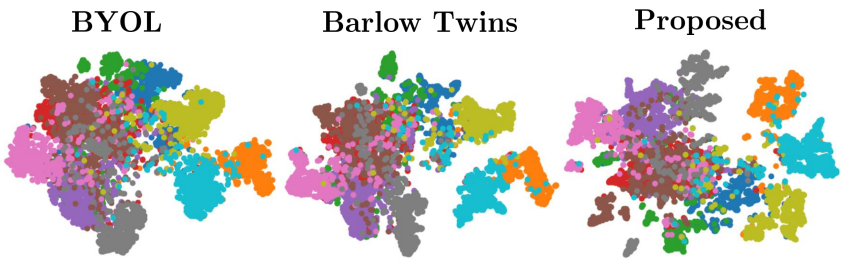

Figure G.3: t-SNE of learned representations for CIFAR10.

follow the evaluation method in (Chen & He, 2021) to stop the algorithms after one hundred epochs. In terms of data augmentation, we use the pipeline of different transformations in Tab. G.5. Note that for the proposed method, we only impose constraint (6c) since our goal here in this task is to extract essential shared information.

We evaluate the proposed method and two AM-SSL baselines as mentioned in the main text, namely, `Barlow Twins` (Zbontar et al., 2021) and `BYOL` (Grill et al., 2020) by feeding the learned representations to a linear classifier. We report both the Top-1 linear classification accuracy and the KNN (with $k = 5$) accuracy. The results are shown in Tab. G.6. One can see that different methods achieve comparable results. The proposed method and `BYOL` attain essentially the same accuracy. The t-SNE (Hinton & Roweis, 2002) visualizations of the test set is plotted in Fig. G.3. One can see that all methods extract "identity-revealing" information to a certain extent, as in the MNIST case.

Remark 1 We should remark that the experiment results suggest that latent correlation maximization (or latent component matching) used in many AM-SSL and DCCA methods works towards the same ultimate goal *under our generative model* in (5). However, this does not suggest that different SSL and DCCA methods are essentially the same in practice—one should not expect that. In fact, there are many factors that affect DCCA and AM-SSL methods' results, e.g., model mismatches, optimization procedure, network construction, and the detailed designs in their loss functions. The difference between the methods normally are more articulated with larger data sets or more complex problems. Nonetheless, our interest lies in theoretical understanding of their common properties, other than the differences in practical implementations. From this perspective, the results in this section support our theoretical analysis in Theorem 1.

G.4 Real Data - More on Validating Theorem 2

Cars3D Data for Cross-sample Generation. In this subsection, we provide more detailed settings and results of the `Cars3D` experiment. To create a multiview dataset, we assume that given the car

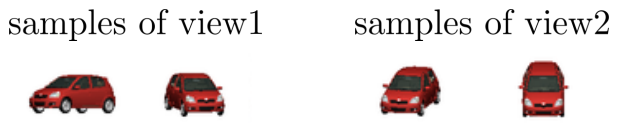

Figure G.4: Samples of the lower elevations (view1) and higher elevations (view2).

Table G.7: Network structures for the Cars3D experiment.

Encoders	Decoders
input: $\boldsymbol{x}_\ell^{(q)} \in \mathbb{R}^{64\times64\times3}$	input: $\boldsymbol{f}^{(q)}(\boldsymbol{x}_\ell^{(q)}) \in \mathbb{R}^{10+2}$
4×4 Conv, 32 ReLU, stride 2	FC 256, ReLU
4×4 Conv, 32 ReLU, stride 2	FC $4\times4\times64$, ReLU
4×4 Conv, 64 ReLU, stride 2	4×4 Conv_Trans, 64 ReLU, stride 2
4×4 Conv, 64 ReLU, stride 2	4×4 Conv_Trans, 32 ReLU, stride 2
FC 256, ReLU	4×4 Conv_Trans, 32 ReLU, stride 2
FC 10+2	4×4 Conv_Trans, 3, stride 2

type that is captured by shared variables $\boldsymbol{z}$ and the azimuths that are captured by $\boldsymbol{c}^{(q)}$, the generation mappings $\boldsymbol{g}^{(1)}$ and $\boldsymbol{g}^{(2)}$ produce car images with low elevations and high elevations, respectively (so they must be different mappings).

We split the car images as follows. We treat the same car model (e.g., a red convertible) with lower and higher elevations as $\boldsymbol{x}_\ell^{(1)}$ and $\boldsymbol{x}_\ell^{(2)}$, respectively. The azimuths are randomly shuffled with different pairs of $\boldsymbol{x}_\ell^{(1)}$ and $\boldsymbol{x}_\ell^{(2)}$. This way, if our generative model holds, $\boldsymbol{z}$, $\boldsymbol{c}^{(q)}$ and $\boldsymbol{g}^{(q)}$ are responsible for 'type', 'azimuth' and 'elevation', respectively. Some samples are shown in Fig. G.4.

Under our splitting, each view has $2\times183\times24 = 8784$ RGB images that all have a size of $64\times64\times3$. We model the 'type' information $\boldsymbol{z}$ using $D = 10$ latent dimensions since many different factors (e.g., color and shape) together give rise to a 'type'. On the other hand, we set $D_1 = D_2 = 2$ to model the 'azimuth' information.

Tab. G.7 shows network structures for the encoders and decoders of our formulation in (F.6). In the table, FC denotes fully connected layer, Conv denotes convolutional layer and Conv_Trans denotes 2D transposed convolutional layer. As before, the structures of $\boldsymbol{\phi}^{(q)}$ and $\boldsymbol{\tau}^{(q)}$ are MLPs with two-hidden-layer and 256 neurons for each layer. For hyperparameters, we set batch size to be $|\mathcal{B}_1| = 100$ and $|\mathcal{B}_2| = 800$, $\beta = 0.1$, $\lambda = 1.0$. For this real data experiment, we also use Adam (Kingma & Ba, 2014) as the optimizer with initial learning rate 0.001 for $\boldsymbol{\theta}$ and 1.0 for $\boldsymbol{\eta}$. We add $\|\boldsymbol{\eta}\|_2^2$ for regularization with parameter 0.0001. We limit the inner loops for solving the $\boldsymbol{\theta}$ and $\boldsymbol{\eta}$ subproblems to 10 epochs as well.

Figs. G.5 and G.6 show more results under the same setting as in Fig. 2 in the main text.

dSprites Data for Cross-sample data Generation. We present the results on an additional dataset, i.e., dSprites (Higgins et al., 2017). In the dSprites dataset, 64×64 images are generated based on five factors: 3 shapes (square, ellipse, heart), 6 scales, 40 orientations, and 32 different horizontal and vertical coordinates.

In particular, we take a subset that contains squares and hearts as the two views of data. In this subset, all the data samples are with the same scale. We assume the generating functions $\boldsymbol{g}^{(1)}$ and $\boldsymbol{g}^{(2)}$ are responsible for the shape of square and heart, respectively. We treat the orientation and horizontal positions as the shared information, i.e., $\boldsymbol{z}$, and the vertical position as the private information $\boldsymbol{c}^{(q)}$. The vertical coordinates are random and not matched between different pairs of $\boldsymbol{x}_\ell^{(1)}$ and $\boldsymbol{x}_\ell^{(2)}$. Overall, we have $40,960$ samples for each view. We set $D = 2$ and $D_1 = D_2 = 1$.

We use the same neural network structure as in Tab. G.7. The only differences lie in the input and latent dimensions. The network structure for $\boldsymbol{\phi}^{(q)}$ and $\boldsymbol{\tau}^{(q)}$ are MLPs with two hidden layers of 128 neurons, and we set $|\mathcal{B}_1| = 100$, $|\mathcal{B}_2| = 500$, $\beta = 0.1$, and $\lambda = 100.0$. Similar as before, we use the Adam (Kingma & Ba, 2014) optimizer with initial learning rate 0.001 for $\boldsymbol{\theta}$. As before, we add

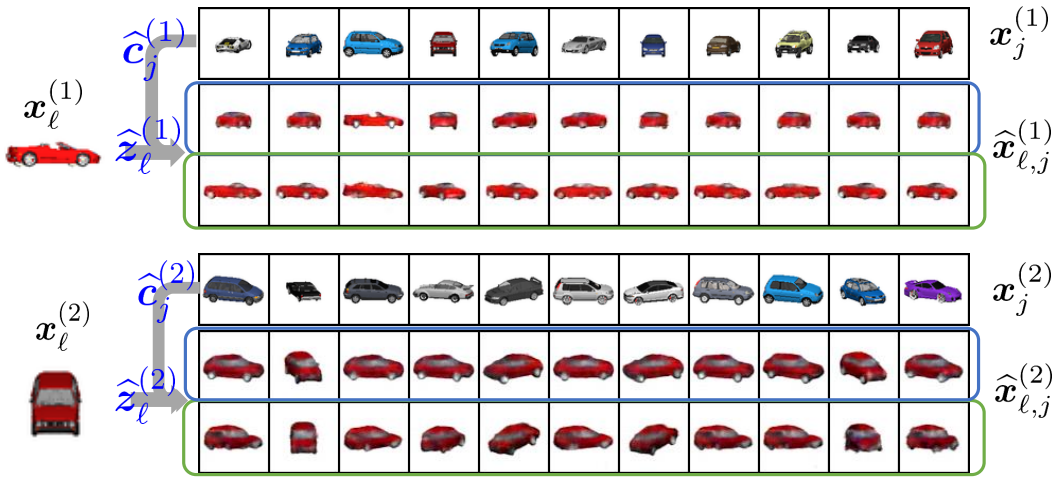

Figure G.5: Generated samples by fixing $\widehat{\boldsymbol{z}}_\ell$ and varying $\widehat{\boldsymbol{c}}_j^{(q)}$; rows in blue boxes are w/ $\mathcal{R}$; rows in green boxes are w/o $\mathcal{R}$.

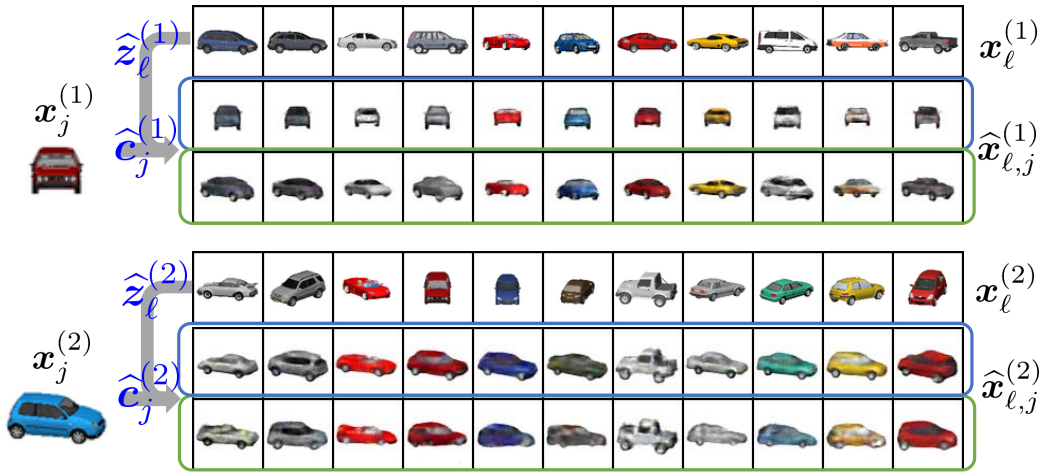

Figure G.6: Generated samples by fixing $\widehat{\boldsymbol{c}}_j^{(q)}$ and varying $\widehat{\boldsymbol{z}}_l$; rows in blue boxes are w/ $\mathcal{R}$; rows in green boxes are w/o $\mathcal{R}$.

a squared ℓ_2 norm regularization on the network parameters $\boldsymbol{\eta}$, and set the regularization parameter to 0.1. We let the inner loop stochastic optimizers run for 10 epochs.

We conduct the same cross-sample data generation experiment as in the Cars3D case. Fig. G.7 shows the results. To be specific, we extract $\widehat{\boldsymbol{z}}_\ell^{(q)} = \widehat{\boldsymbol{f}}_{\mathrm{S}}(\boldsymbol{x}_\ell^{(q)})$ that represents the rotation and horizontal coordinate information and $\widehat{\boldsymbol{c}}_j^{(q)} = \widehat{\boldsymbol{f}}_{\mathrm{P}}(\boldsymbol{x}_\ell^{(q)})$. And we combine this information together to generate synthetic samples $\widehat{\boldsymbol{x}}_{\ell,j}^{(q)}$ with the learned reconstruction network $\boldsymbol{r}^{(q)}$, i.e., $\widehat{\boldsymbol{x}}_{\ell,j}^{(q)} = \widehat{\boldsymbol{r}}^{(q)}([(\widehat{\boldsymbol{z}}_\ell^{(q)})^\top, (\boldsymbol{c}_j^{(q)})^\top]^\top)$.

The observations are similar to that in the Cars3D experiments. *Ideally, the generated samples should have the rotation and horizontal position of $\boldsymbol{x}_\ell^{(q)}$ (contained in $\widehat{\boldsymbol{z}}_\ell^{(q)}$) while the vertical position of $\boldsymbol{x}_j^{(q)}$ (contained in $\widehat{\boldsymbol{c}}_j^{(q)}$).* One can see that without using the independence regularizer $\mathcal{R}$, the generated samples may have rotation change, shape deformation compared to $\boldsymbol{x}_\ell^{(q)}$ or simply the

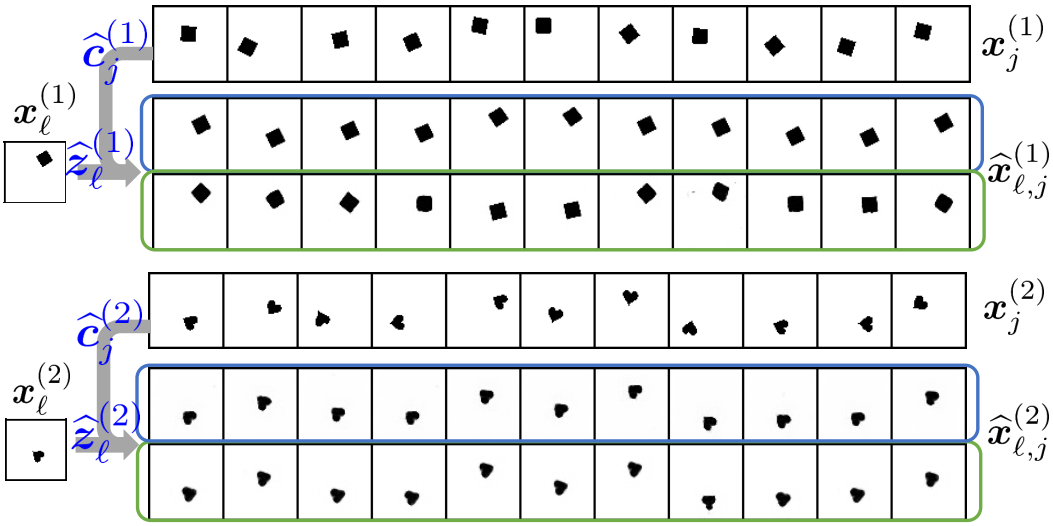

Figure G.7: Generated samples by fixing $\widehat{\boldsymbol{z}}_\ell$ (rotation and horizontal position) and varying $\widehat{\boldsymbol{c}}_j^{(q)}$ (vertical position). Top: the square view; bottom: the heart view; rows in blue boxes are w/ $\mathcal{R}$; rows in green boxes are w/o $\mathcal{R}$.

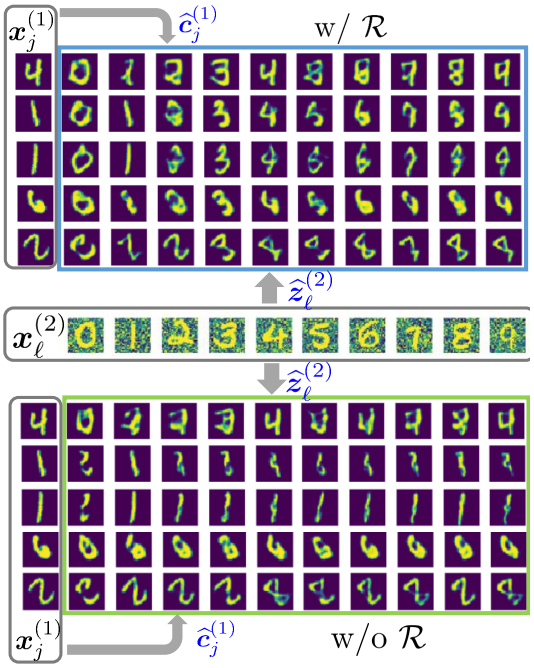

Figure G.8: Cross-view generation from $\boldsymbol{x}_\ell^{(2)}$ to $\boldsymbol{x}_\ell^{(1)}$.

vertical position is not exactly replicated from the sample $\boldsymbol{x}_j^{(q)}$. However, with the $\mathcal{R}$ regularization, the results are exactly what one expects to see. This again verifies our claim in Theorem 2.

Multiview MNIST Data for Cross-view Generation. Using the multiview MNIST data, we also show the cross-view generation results in Fig. G.8. Here, we extract $\widehat{\boldsymbol{z}}_\ell^{(2)} = \widehat{\boldsymbol{f}}_{\mathrm{S}}^{(2)}(\boldsymbol{x}_\ell^{(2)})$ from the second view and $\widehat{\boldsymbol{c}}_j^{(1)} = \widehat{\boldsymbol{f}}_{\mathrm{P}}^{(1)}(\boldsymbol{x}_j^{(1)})$ from the first. Then, we generate $\widehat{\boldsymbol{x}}_{\ell,j}^{(1)} = \widehat{\boldsymbol{r}}^{(1)}([(\widehat{\boldsymbol{z}}_\ell^{(2)})^\top, (\boldsymbol{c}_j^{(1)})^\top]^\top)$ shown in the blue and green boxes. *Ideally, the generated samples should have the digit information*

of $\boldsymbol{x}_\ell^{(2)}$ *(contained in* $\widehat{\boldsymbol{z}}_\ell^{(2)}$*) while the style information of* $\boldsymbol{x}_j^{(1)}$ *(contained in* $\widehat{\boldsymbol{c}}_j^{(1)}$*).* Clearly, using $\mathcal{R}$ attains the desired results. Note that this dataset is challenging as the noise in view 2 is very high, making it hard to achieve perfect matching and reconstruction—but our result is still plausible.